Università degli Studi di Napoli Federico II
Dipartimento di Strutture per l'Ingegneria e l'Architettura

Giuseppe La Manna Ambrosino

SEISMIC PERFORMANCE OF DUAL - STEEL ECCENTRIC-BRACED FRAMES IN SIMPLE AND DUAL CONFIGURATION

Tesi di Dottorato
XXVI ciclo

Il Coordinatore
Prof. Ing. Luciano ROSATI

Dottorato di Ricerca in Ingegneria delle Costruzioni

"*La cosa brutta del dottorato è che quando in dipartimento ti senti davvero a casa, è arrivato il momento di andare via*" con questa frase mi accolse una cara collega, quando iniziai il dottorato. Aveva perfettamente ragione!

E proprio come in una grande famiglia, in questi anni ognuno mi ha dato qualcosa, ognuno ha arricchito la mia persona, ad ognuno devo dire grazie.

Il prof. Landolfo mi ha insegnato che non basta avere ruolo di responsabilità per essere un buon leader, e che non serve alzare la voce per coordinare un gran numero di persone. I tutti questi anni non l'ho mai sentito alzare la voce, neppure una volta. Il suo rispetto per la persona fa di lui un Leader speciale. Ha saputo spronarmi nell'ultimo tratto, quello più duro, quando era più facile mollare che andare avanti; gliene sarò sempre grato.

A Mario dico semplicemente Grazie. Lui può coglierne perfettamente il reale significato. Ha pazientemente sopportato il mio essere "San Tommaso", ha stimolato la mia curiosità scientifica, mi ha ascoltato da Amico Fraterno.

A tutti gli allievi dico due volte grazie, soprattutto a quelli più scalmanati, a quelli più disinteressati. Le lezioni, le correzioni, gli esami credo davvero che abbiamo dato più a me che a loro. La mia prima lezione è uno dei ricordi più belli che conservo.

Il trasferimento della conoscenza dovrebbe essere il fine ultimo della ricerca!

Adesso dovrei elencare colleghi ed amici che mi hanno accompagnato in questo percorso, ma temo di essere pedante, o addirittura stucchevole. Con molti di loro ho un rapporto speciale, in questi anni abbiamo riso, ci siamo raccontati sogni e paure, abbiamo discusso, semplicemente siamo cresciuti insieme.

"Regola numero uno: mai fidarsi di un universitario!" con questa frase mi accolse un caro collega, quando iniziai il dottorato. Aveva perfettamente torto!

Dedico questo lavoro di tesi a mia madre Annamaria.
"Hai sacrificato i tuoi studi e il tuo lavoro per la Famiglia
e solo oggi, forse, riesco a capirne il senso,
questo Dottorato è il tuo"

A mio padre Giovanni.
"potrei lasciare questa pagina completamente bianca,
capiresti perfettamente"

A Linda, Paolino e Stefania
i miei affetti più cari

"La vera misura di un uomo si vede da come tratta qualcuno
da cui non può ricevere assolutamente nulla in cambio"
(Samuel Johnson)

"A cosa sarà servito avere le mani pulite,
se le avremo tenute in tasca?"
(Don Lorenzo Milani)

SOMMARIO

Lo studio sintetizzato in questa tesi è volto ad investigare la risposta sismica di strutture di acciaio a controventi eccentrici sia in configurazione semplice che duale (ovvero in accoppiamento con telai momento-resistente) progettati con l'uso combinato di acciai ad alta resistenza ed acciai dolci di tipo tradizionale. In particolare, nella prima parte della tesi sono stati dapprima affrontati gli aspetti prettamente progettuali e di verifica. Nella seconda parte è stato condotto uno ampio studio numerico su un insieme di strutture di riferimento analizzando l'influenza di un vasto spettro di parametri, quali il numero di piani, la lunghezza delle campate, il tipo di acciaio ad alta resistenza, la tipologia delle colonne ed il terreno di fondazione. L'analisi dei parametri che caratterizzano la prestazione strutturale ha consentito di proporre criteri di progetto alternativi a quelli attualmente codificati. Nella terza parte della tesi, sulla scorta dei risultati ottenuti dalle analisi parametriche, è stato condotto lo studio preparatorio per la programmazione di prove sperimentali su scala reale di un edificio in acciaio prototipo con la finalità di studiare la capacità di ricentraggio, che la parte a telaio può offrire in una struttura con schema duale con controventi eccentrici e link removibili.

ABSTRACT

The work summarized in this thesis is devoted to investigate the seismic response of eccentric braced frames in simple and dual configuration (namely structural systems made of moment-resisting frames in parallel with braced frames) designed with the combined use of high strength steel (HSS) and of mild carbon steel (MCS). In particular, the first part of the thesis concerns the issues related to both design and verification check. In the second part, a wide and comprehensive parametric study is described and discussed in order to characterize the performance of an ensemble of reference buildings. To this aim, several design parameters are examined, such as: the number of storeys the length of bays, the grade of steel, the steel column sections and the soil foundation. The results from both nonlinear static and incremental dynamic analyses are presented and discussed thus allowing to draft novel design to improve the seismic performance of the examined structural typology. In the third part of the thesis, on the basis of the numerical results obtained from the parametric study, a preparatory study addressed to design the experimental setup for a real scale steel building made of dual Eccentric braced frame having removable links. The aim is to investigate the recentering capacity that the moment resisting spans may provide.

TABLES OF CONTENTS

1 INTRODUCTION

1.1 FRAMEWORK

The study summarized within this thesis is mainly addressed to investigate the seismic performance of dual steel eccentric braced structures in simple and dual configuration. The whole research activity has been carried out within two international research projects, that are (i) the European research project of the Research Fund for Coal and Steel RFSR-CT-2009-00024 "High Strength Steel in Seismic Resistant Building Frames", (ii) Duarem "Full-scale experimental validation of dual eccentrically braced frame with removable links" (7 EU Framework).
Both research projects are strictly correlated. Indeed, the former focused on the seismic performace of frames designed with the combined use of high strength steel (HSS) for non-dissipative members and of mild carbon steel (MCS) for dissipative members. The second focused on the design of dual eccentric braced frames in order to verify the effectiveness of the re-centring capability using removable seismic links.

1.2 OBJECTIVES

The main objectives of this work are:

- to investigate on the use of High Strength Steel in seismic resistant structures, focusing on the dual steel concept;
- to assess the dual steel concept applied to eccentric braced frames in simple and dual configuration;
- to develop design criteria and performance based design methodology for dual-steel structures using high strength steel;
- to investigate on design parameters (i.e. behaviour factor q, overstrength factor) to be implemented in further versions of the seismic design code (EN 1998-1);

- to investigate on the re-centering capability of dual structures with removable dissipative links;
- to analyse the behaviour and the interaction between the steel frame and the reinforced concrete slab in the link region;

1.3 OUTLINE OF THE THESIS

In Chapter 2, some general information regarding high strength steel are provided, relating to applications and gains, production. Then a short description of dual steel concept is given.
In Chapter 3, EBF systems in simple and dual configurations are described; particularly the seismic response and link model are deeply discussed.
In Chapter 4, the assumptions and the main results of a numerical parametric study are described and discussed in order to examine the seismic performance and design aspects of ebf system in simple and dual configuration designed with the combined use of Hss and mild grade steel.
In Chapter 5, a full scale steel building prototype with dual-ebf system with removable link is described. In detail the re-centering capability of a MRFs combined with EBFs, and possibility of replace the link element after earthquake events are investigated in order to design a real scale mock-up.
In Chapter 6 the conclusions are presented.

2 HIGH STRENGTH STEEL AND DUAL STEEL CONCEPT

2.1 INTRODUCTION

The material that we know as modern steel has evolved from ancient iron-making techniques, then in the course of time it evolved and changed its chemical properties, metallurgical structures and weldability. So that the current steel is very different from the iron that was used for the earliest application. In the course of time, a growing request of most excellent mechanical property implied an increasingly attention on the part of metallurgic industry, steel fabricators, researchers and designers (Bjorhovde, 2004).
The efficiency of steel structural members and connections and the seismic performance of steel structures can be improved in many cases by using steels with high values of yield stress and/or tensile strength, even if the use of high strength steels (HSSs) belong to machine, automotive and aeronautical fields too, and not only to civil applications. (Vulcu, 2013).
During last decades, high strength steels have gained ground in the field of steel market, and the steel grade S355 that until 20 years ago was considered an high strength steel, today is the more used steel grade for hot rolled plates and H-sections.

2.2 APPLICATIONS AND GAINS OF HSS

In recent years, significant development in steel processing occurred. Indeed, the improvements in industrial processes by the combination of rolling practices with and cooling rates allowed obtaining high strength

steel (HSS) with very attractive properties. Owing to the high performance, the use of HSS has a number of benefits in terms of economic, architectural, environmental and safety (Samuelsson et al., 2005)

Referring to economic aspects by increasing the strength of steel, the structural sections can be reduced; so this may reduce the weight of the structure and the volume of weld metal, and consequently the total costs linked to the fabrication, erection and foundation system. In the figure 2.1 is depicted the reduction of wall thickness and weight with increasing strength of steel while in the fig. 2.2 is depicted the ultimate loads for columns with increasing strength of steel.

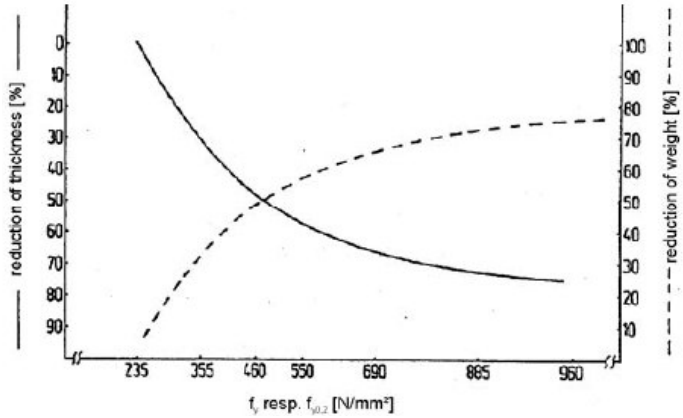

Fig. 2.1 - Reduction of thickness and weight with increasing strength of steel.

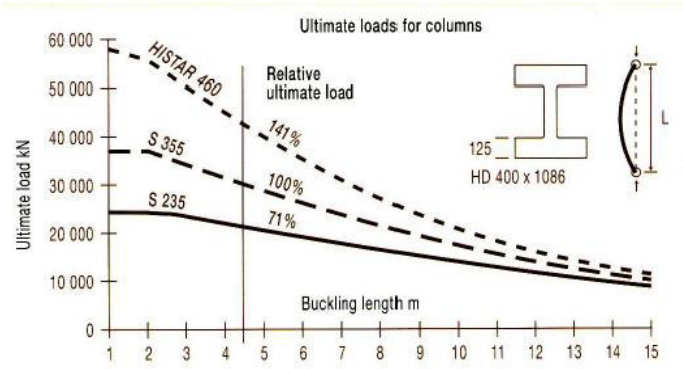

Fig. 2.2 - The ultimate loads for columns with increasing strength of steel.

From an architectural point of view the size of structural elements can be reduced enabling special aesthetic and elegant structures, which embed in the environment in an outstanding manner. Then, the use of a HSSs produced great beneficial in term of sustainability, in fact less steel consumption means reduced consumption of raw materials, reduced emissions and energy, finally it reduces the CO_2 emissions; furthermore steel is the world's most recycled material as well is indicated in the fig. 2.3.

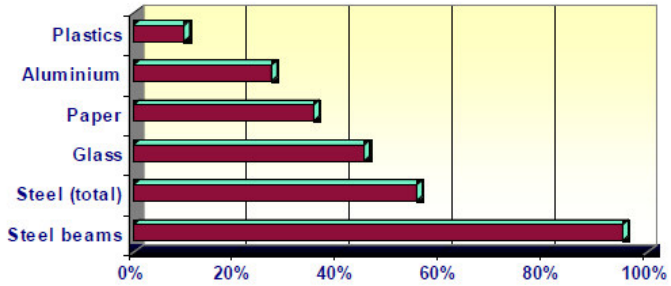

Fig. 2.3 - Comparison of world's most recycled material.

Finally, also in term of safety, high strength steels combine high values of strength with excellent toughness properties so that a high safety both in fabrication and application of the structures is applied. For safety control by design it is compulsory to ensure constant mechanical properties. From this point of view, compared to MCS, HSS are really performant such as in fig. 2.4.

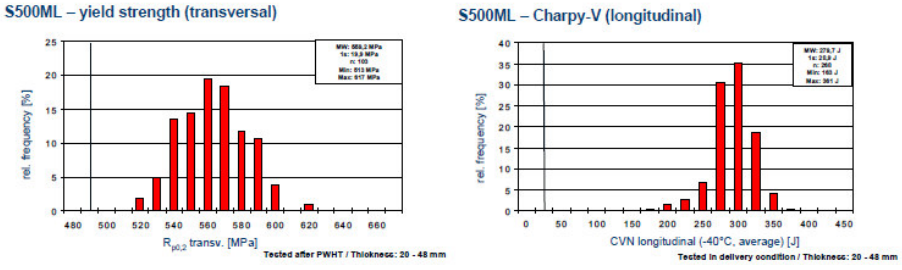

Fig. 2.4 - Mechanical properties.

2.3 HIGH STRENGTH STEEL PRODUCTION

The mechanical properties of steel are related to its chemical composition and its microstructure, meaning the displaying pattern and the chemical composition of the micro crystals that compose the steel. This micro-structure depends mainly on both the chemical composition and the thermal treatment. By increasing the content of alloy elements, an increase in the resistance of steel is obtained and at the same time a reduction of weldability and ductility. Then, if weldable steel is required, the content of alloy elements must be situated between relatively restricted boundaries.
Another solution, to increase the resistance without reduce the ductility and weldability, is to apply thermal treatment and the temperature control during rolling. A few procedures are used generally for improving the resistance of the steel elements, among which the last two on a larger scale:

- Steel normalizing (N): the strength of normalized steel is mainly given by the alloy elements and not by the microstructure; if an adequate control of the temperature is ensured during rolling, further normalization is not necessary; in the classic manufacturing procedure, the steel is normalized (heated up to 920-930ºC and then slowly cooled) in order to improve it's mechanical characteristics, especially.
- Thermo-mechanical steels (TM): the resistance of thermo-mechanical steels is mainly given by the microstructure; the alloy content is lower in comparison to normalized steels.
- Hardening thermal treatment followed by regression to high temperature (QST): this is a thermal process in which the steel, after being heated, is rapidly cooled in water (quenching) in order to achieve an increase in strength, then it is heated in order to obtain a finer granulation and a better ductility and weldability; the improvement treatment is applied in most cases to steels with the yield limit between 420 N/mm^2 and 690 N/mm^2.

Due to the lack of plastic properties, quenched steel cannot be used in steel structures. For this reason it is subjected to a supplementary thermal treatment called reheating. By reheating, a finer granulation is obtained and also a more uniform distribution of the mechanical properties. The carbon from the martensite diffuses in the ferrite mass

and forms iron carbides; by reheating the quenched steel has a lower toughness and tensile strength but the elongation increases.
The mechanical properties of quenched and reheated steel are superior to the steel that is not terminally treated, i.e. the lower the reheating temperature the higher the mechanical resistances, and the elongation smaller.
In steels that have been subjected to quenching and reheating, the value of the yield limit and of the tensile strength is closer together; if for the steels that have not been thermally treated the ratio has values between 0.65 and 0.7, for improved steels this ratio rises to values between 0.8 and 0.9 (sometimes even higher); the ratio is even closer to unit value as the reheating temperature is lower and decreases as these increases.
Due to the fine crystalline and uniform structure obtained by improvement, low alloy improved steels present superior toughness properties compared to low alloy normalized steels, especially in the domain of low temperatures; the elements of low alloy improved steels can be welded considering some special conditions.
In the last years in the USA lead to the so called Advanced High Strength Steels (AHSS) and Ultra High Strength High Toughness Steels, characterised by tensile strengths of f_u >1000 N/mm^2, designed for the automobile industry, having the form of thin sheets. In Europe, hot rolled profiles (IPE, HEA, HEB, and HEM) are produced also from S460 steel grade.

2.4 DUAL STEEL CONCEPT

Seismic applications potentially represent the rational field to exploit the high performance of HSS. In fact, according to modern codes, the seismic design of steel or composite buildings are based on the concept of capacity design, where specific zones of the structures should be able to develop plastic deformation in order to dissipate the seismic energy. On the contrary, the non-dissipative zones and members should behave elastically under seismic action in order to avoid the brittle collapse of the building. For this reason, these zones should be designed to resist the full plastic strength of the dissipative members. So, the large overstrength demands to non-dissipative zones lead to high material

consumption, and sometimes, huge size of members to fulfill this design requirement.

The combined use of HSS for non-dissipative members and of mild carbon steel (MCS) for dissipative members may allow an easier application of capacity design criteria. The expected design improvement would be obtained in terms of smaller member sizes than those obtained when using MCS only. Structures designed using the combination of HSS and MCS are termed "dual-steel" structures.

Recent studies (Dubina et al. 2006, Dubina et al. 2008, Dubina 2010) have highlighted the advantages of dual-steel concept, especially for what concerns the control of seismic response of multi-storey buildings to achieve overall ductile mechanism.

REFERENCES

- Bjorhovde R. (2004). Development and use of high performance steel - *Journal of Constructional Steel Research*, 60, 3-5: 393-400
- Vulcu M.C. (2013). *Seismic performance of dual steel frames of cfrhs and welded beam-to-column joints. Phd Thesis*. Timisoara: Editura Politehnica
- Samuelsson A., Schröter F. (2005). High performance steels in Europe - Production processes, mechanical and chemical properties, fabrication properties. *Use and application of high performance steels for steel structures. Zurich: IABSE*
- Dubina D, Dinu F, Zaharia R, Ungureanu V, Grecea D. (2006) Opportunity and effectiveness of using high strength steel in seismic resistant building frames, *International Conference in Metal Structures*;
- Dubina D, Stratan A, Dinu F. Dual. (2008). High-strength steel eccentrically braced frames with removable links. Earth Eng Struct Dyn
- Dubina D. (2010) Dual-steel frames for multistory buildings in seismic areas, In: *Internacional Colloquium Stability and Ductility of Steel Structures*.

3 ECCENTRIC BRACED FRAMES IN SIMPLE AND DUAL CONFIGURATION

3.1 ECCENTRIC BRACES

The eccentric braced frame (EBF) is a hybrid lateral force-resisting system. In fact, it's obtained by the combination of two different framing systems: the moment-resisting frame and the concentrically braced frame. EBFs can combine the main advantages of each conventional framing system and minimize their respective disadvantages, as well. In general EBFs possess high elastic stiffness, stable inelastic response under cyclic lateral loading, and excellent ductility and energy dissipation capacity.

Research on the behaviour of EBFs started in the second mid-1970s (Roeder & Popov 1977, Roeder & Popov 1978) and continued up today. All these studies confirmed the reliability of EBFs to resist horizontal actions. Eccentrically braced frames in buildings typically include the use of shear links, which are sections of beams that yield and plastically deform in shear, to provide a stiff and ductile lateral load resisting system.

Shear links in eccentrically braced frames have been studied for new buildings (Kasai & Popov 1983, Popov & Malley 1983, Hjelmstad & Popov 1986, Ricles & Popov 1987, Engelhardt & Popov 1989), but their use is now also becoming a viable method to retrofit RC structures and for protecting bridges. Two examples of bridge retrofitting are Richmond San Rafael Bridge (Itani 1997) and the use of shear links in the tower of the new San Francisco-Oakland Bay suspension cable bridge (Nader et al. 2002).

Figures 3.1 to 3.2 show some examples of structures with EBF systems designed to resist horizontal actions.

a)  b) 

Fig. 3.1. Multi-story building with EBF system, San Diego (USA).

a)  b) 

Fig. 3.2. Multi-story building with EBF system, Alikahya (Turkey).

a)  b) 

Fig. 3.3 Istanbul Bilgi University, Prep School Building (Turkey).

3.2 STATIC BEHAVIOUR OF EBS

The key distinguishing feature of an EBF is that at least one end of each brace is connected so as to isolate a segment of beam called "link". EBF arrangements, usually adopted, are shown in Fig. 3.4. In each framing scheme of Fig. 3.5 the links are identified by a bold segment. The four

EBF arrangements here presented are usually named as split-K-braced frame, D-braced frame, V-braced and finally inverted-Y-braced frame.

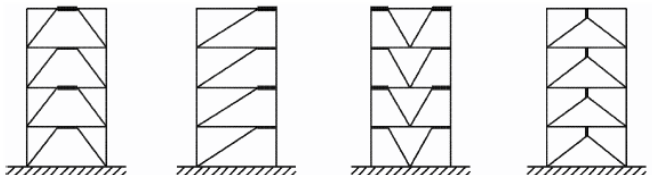

Fig. 3.4. EBs configuration.

The static behaviour of EBs is deeply influenced by the link. The inelastic action is restricted in the links in order to keep the framing around in the elastic range by making them able to sustain the maximum forces that the links can develop. In this way the links act as ductile seismic fuses and preserve the integrity of the whole frame. For this reason the other components of the framing system (such as diagonal braces, columns and link connections) should be designed for the forces generated by the full yielding and strain-hardening of dissipative links. To do this it is important to explicate the distribution of internal actions in an EBF system and define a relationship between frame shear force and link shear force. This relationship depends only on the EBF configuration, in fact it is the same if the link response is elastic or plastic. The design actions in links can be calculated using equilibrium concepts. For example in a split-K-braced EBF (shown in Fig. 3.5), assuming that the moment at the center of the link is equal to zero, the link shear force V can be expressed as:

$$V = \frac{F \cdot H}{L} \qquad (3.1)$$

where F is the lateral force, H is the interstory height and L is the bay length.

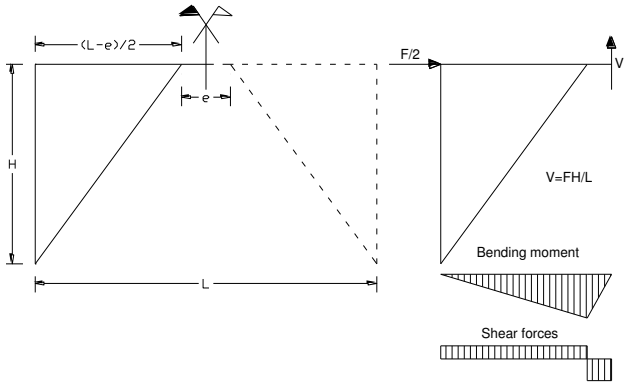

Fig. 3.5. Design action in link for a split-K-EB configuration.

In case of an inverted-Y-braced EBF (Fig. 3.6), assuming that the moment at the brace connections is equal to zero (i.e. in case of pinned braces), the link shear force V can be expressed as:

$$V = F \tag{3.2}$$

where F is again the lateral force.

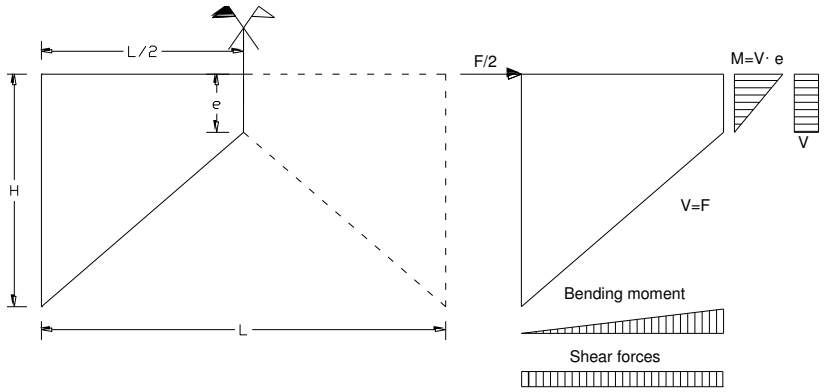

Fig. 3.6 Design action in link for an inverted-Y-EB configuration.

3.3 KINEMATIC OF PLASTIC MECHANISM OF DUCTILE EB SYSTEMS

An important aspect is the kinematic of plastic mechanism of the EB systems. In fact, in the design of a seismic resistant EB, it is necessary to

estimate the plastic rotation demand on the links. In particular the relationship between story plastic drift angle and link plastic rotation is the main topic. This relationship can be simply derived by assuming the frame outside the link as rigid (because the elastic deformation in the frame outside the link is small if compared with the link plastic deformation), thus depending only on configuration of EBs and geometrical proportions, assuming the inextensibility and rigid plastic behaviour of members. Link rotation is denoted by the symbol γ to remind the importance of shear yielding in link rotation.

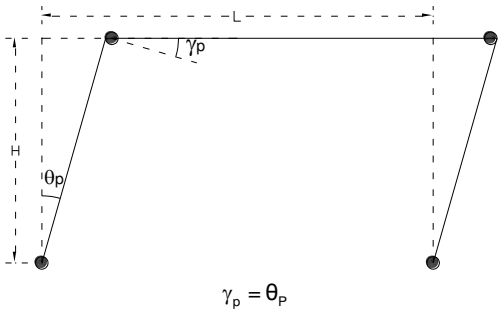

Fig. 3.7. Kinematic of a moment resisting frame.

In case of a moment resisting frame (MRF), the kinematic of plastic mechanism is very simple and the relationship between the story drift angle and the plastic rotation of dissipative parts is given in Fig. 3.7.

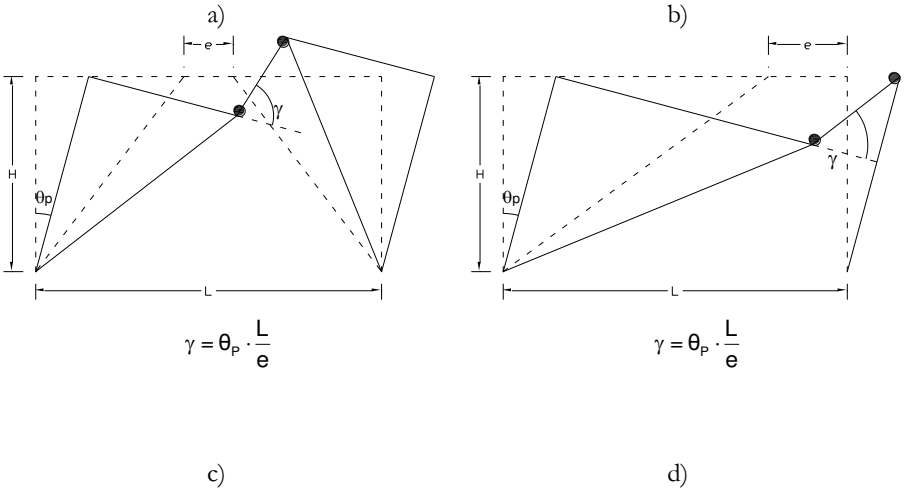

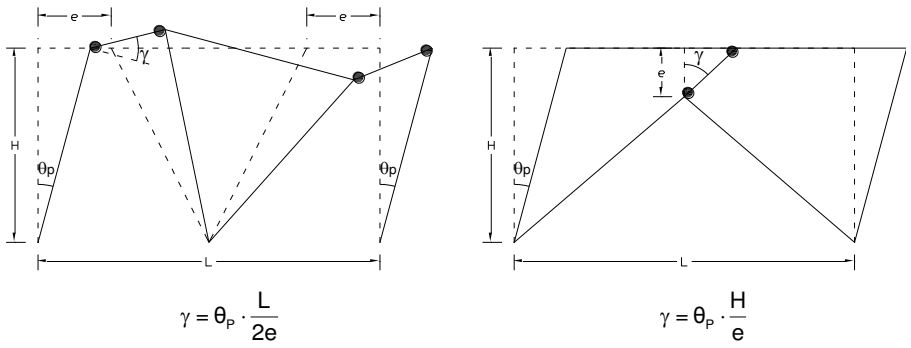

Figure 3.8. Kinematic of plastic mechanism of several EB configurations: split-K-braced frame (a); D-braced frame (b); V-braced frame (c); inverted-Y-braced frame (d).

Figure 3.9 shows a plot of link rotation demand versus the ratio L/e for a split-K-EB. This plot clearly shows that plastic rotation demand is larger in EB systems than in a MRF (where $L/e = 1$). The link rotation demand grows as the link length decreases. This plot demonstrates that links should not be too short, because the rotation demand may become excessive.

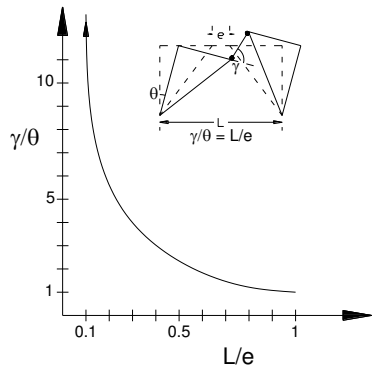

Fig. 3.9 Variation of link rotation demand with e/L ratio.

3.4 LINK MECHANICAL BEHAVIOUR

Besides the kinematic of plastic mechanism, another important aspect characterizing the EB inelastic behaviour is the cyclic hysteretic response of shear links. Fig. 3.10 clearly shows that shear links can provide stable and well rounded hysteresis loops, which indicate a large energy dissipation capacity.

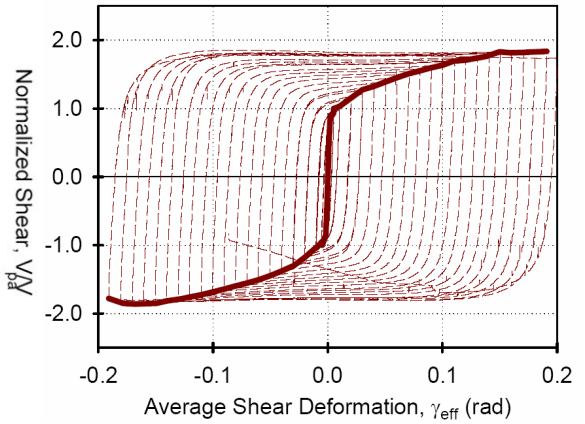

Fig. 3.10. Shear link hysteretic response.

Three different domains characterize the link behaviour (Kasai & Popov, 1986): elastic, pre-buckling inelastic and post-buckling, bounded by three limit states: yield, buckling and failure. The inelastic pre-buckling behaviour is characterized by remarkable cyclic stability of the hysteresis loop and an active link functions most effectively as an energy damping system. After the web buckling, the link continues to dissipate energy. However, the predominant load carrying mechanism changes and therefore so does the way of dissipating energy. The post-buckling energy dissipation mechanism, based on the tension-field, is less efficient than the pre-buckling one. Failure of a link is defined as complete inability to sustain load, and is generally caused by low-cycle fatigue in highly localized regions which experience extreme strain reversals due to the cyclic changing of the buckled mode shape (Hjelmstad et al., 1983).
Link inelastic performance essentially depends on its length and cross-section properties. For a given cross-section, the link length controls the yielding mechanism and the ultimate failure mode. Short links are mainly dominated by a shear mechanism, instead flexure controls link response

for long links. Moreover intermediate links are characterized by a *M-V* interaction.
Assuming perfect plasticity, no flexural-shear interaction and equal link end moments, the theoretical dividing point between a short link (governed by shear) and a long link (governed by flexure) is a length of $e = 2M_p/V_p$, where the plastic bending moment $M_p = Z \cdot f_y$ (in which Z is the plastic modulus and f_y is the value of steel yielding stress) and $V_p = 0.55 \cdot \left(d - 2t_f\right) \cdot t_w \cdot f_y$ (in which d is the depth of the cross section and t_w is the web thickness). A large number of experimental activities (such as Kasai & Popov 1986, Hjelmstad & Popov 1983, Foutch 1989) indicate that the assumption of no M-V interaction is reasonable, but an assumption of perfect plasticity is not correct. In fact, substantial strain hardening occurs in shear links. According to tests performed on American wide-flange steel profiles, the average ultimate link shear forces reach the value of $1.5V_p$. One implication of this strain hardening is that both shear and moment yielding occur over a wide range of link lengths. In case of shear links, end moments substantially greater than M_p can be developed. In fact, shorter is the link, greater the bending moment will be in order to necessarily have $V = 2M/e$. The large end moments, combined with the significant strain gradient that occurs in links, lead to very large flange strains, which in case of steel built up sections can prompt the flange welds failure. Kasai and Popov (1986) estimated that the maximum link end moments can be assumed $1.2M_p$. Thus, from link static of Fig. 3.6, if the end moments are limited to $1.2M_p$ and the link shear is assumed to reach $1.5V_p$, the limiting link length is $e = \frac{2 \cdot (1.2M_p)}{1.5 \cdot V_p} = 1.6\frac{M_p}{V_p}$.
Then the following equations can be used to classify the link mechanical response:

Shear (short) links: $$e \le 1.6\frac{M_p}{V_p} \qquad (3.3)$$

Intermediate links: $$1.6\frac{M_p}{V_p} < e < 2.5\frac{M_p}{V_p} \qquad (3.4)$$

Flexure (long) links: $e \geq 2.5 \frac{M_p}{V_p}$ (3.5)

The ultimate failure modes of short and long links are quite different. In particular inelastic web shear buckling is the ultimate failure mode of short links. This buckling mode can be delayed by adding web stiffeners (Fig. 3.11).

a)  b) 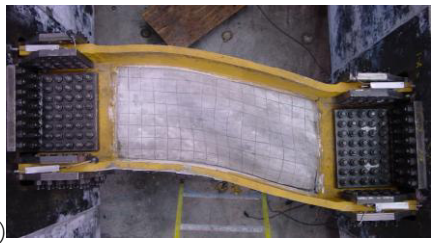

Fig. 3.11. Plastic deformation of short links: inelastic response of stiffened short link (a); inelastic response of unstiffened short link (b).

Hjelmstad & Popov (1983) developed several cyclic tests in order to relate the web stiffeners spacing to link energy dissipation, and Kasai & Popov (1986) subsequently developed simple rules to relate stiffeners spacing and maximum link inelastic rotation γ up to the web buckling. Starting from the consideration that the link web buckling modes are very similar to the ones of plates under shear loading they applied the plastic plate shear buckling theory to relate the stiffeners spacing to the maximum deformation angle of a shear link. In fact the theoretical plastic buckling shear stress τ_b was obtained starting from the elastic buckling solution τ_E and can be expressed as:

$$\tau_b = \eta \cdot \tau_E \quad (3.6)$$

where η is a plastic reduction factor, that is a function of plate strain hardening history and it was experimentally derived, while the elastic buckling shear stress τ_E can be expressed as:

$$\tau_E = \frac{\pi^2 E}{12\left(1 - \nu^2\right)} K_S(\alpha) \cdot \left(\frac{1}{\beta}\right)^2 \quad (3.7)$$

in which ν is the Poisson ratio, k_s is a plate buckling coefficient, which is a function of the aspect ratio a and the boundary conditions, that are

assumed in this case as clamped end conditions. In particular the aspect ratio is equal to $\alpha = a/b$, where a is the stiffener spacing and b is the web panel height, while β is the web panel height-to-thickness ratio that is equal to $\beta = b/t_w$, where t_w is the web thickness.

The secant shear modulus G_s (Gerard 1948 and 1962) for the shear link was defined as:

$$G_S = \frac{\tau}{\bar{\gamma}} \tag{3.8}$$

in which $\bar{\gamma}$ is the maximum shear deformation angle attained preceding the web buckling, which has to be experimentally measured, and τ is the corresponding shear stress approximately defined as $\tau = V/A_w$, where V is the shear force and A_w is the web area.

It was found that there is a linear relationship between η and the ratio G_S/G, in which G is the elastic shear modulus given by $G=E/2(1+\nu)$, where E is the Young's modulus and ν=0.3. Hence, this relationship is expressed by:

$$\eta = 3.7\frac{G_S}{G} \tag{3.9}$$

Substituting Equations 3.8 and 3.9 into Equation 3.6 with $\tau = \tau_b$ at an incipient buckling stage it results:

$$\tau_b = 3.7\frac{\tau_b}{\bar{\gamma}G}\cdot\tau_E \tag{3.10}$$

that can be rearranged leading to:

$$\bar{\gamma} = \gamma_b = 3.7\frac{\tau_E}{G} \tag{3.11}$$

Then using Equation 7, Equation 11 gives:

$$\gamma_b = 8.7K_S(\alpha)\cdot\left(\frac{1}{\beta}\right)^2 \tag{3.12}$$

Furthermore, instead of using the parameter β it is more convenient to approximate it by a beam depth to web thickness ratio d/t_w . Also, since it has been pointed out that the web stiffeners are effective in reducing the possibility of lateral torsional buckling (Hjelmstad & Popov 1983), a maximum spacing of a/d=1 is adopted. Considering these factors, for

the range of γ from 0.03 to 0.09 radians, Equation 3.12 can be conservatively approximated as:

$$\frac{a}{t_w} + \frac{d}{5t_w} = C_B \qquad (3.13)$$

where the constant C_B is equal to 56, 38, and 29, respectively for γ equal to 0.03, 0.06 and 0.09 rad. Thus rearranging Equation 3.13, it was possible to draw the following simple expressions for each required link deformation capacity (Kasai & Popov 1986):

$$a = 29t_w - \frac{d}{5} \qquad \text{for } \gamma = 0.09 \text{ radians} \qquad (3.14)$$

$$a = 38t_w - \frac{d}{5} \qquad \text{for } \gamma = 0.06 \text{ radians} \qquad (3.15)$$

$$a = 56t_w - \frac{d}{5} \qquad \text{for } \gamma < 0.03 \text{ radians} \qquad (3.16)$$

where a is the distance between equally spaced stiffeners, d is the link depth and t_w is the web thickness.

In order to study the effect of inelastic web buckling in links, Popov & Engelhardt (1988) reported the results of two series of cyclic tests on both stiffened and unstiffened isolated links. In the first series fifteen full-size shear links were subjected to equal end moments to simulate the performance of a typical link in a split-K-braced frame. In this case the unstiffened links manifested severe web buckling shortly after yielding, hence their load-carrying capacity rapidly reduced. The specimens provided with stiffeners equally spaced on both link side according to Equation 3.14 showed a significant improvement in performance, achieving large inelastic rotations with full rounded hysteretic loops, confirming a plastic rotation capacity of about 0.10 radians under cyclic excitation and 0.20 radians under monotonic loading. In the second series shear links were subjected to unequal end moments in order to simulate the performance of links located next to a column. In fact, in this configuration the typical ratio of elastic end moments can be on the order of 2 to 4 or more. If steel behaved as a perfectly plastic material, the equalization of link end moments could occur if the link is loaded to its ultimate state. However, because of steel strain hardening, this end

moment equalization may not occur. The tests conducted on links with unequal end moments permitted to understand that:

1) for very short links, i.e. $e \leq M_p/V_p$, unequal end moments remain unequal throughout the loading history up to link failure. The ultimate link end moment at the column face is significantly larger than the predicted equalized moment. As link length increases, the ultimate link end moments tend to equalize. In particular, when link length is about $e \geq 1.3M_p/V_p$, full equalization of end moments can occur.

2) The initial unequal end moments have little effect on the plastic rotation capacity and on the overall hysteretic behaviour.

3) Interaction between bending moment and shear force can be neglected when predicting the yield limit state of a link. In fact, even in the presence of high shear force, the full plastic moment can be assumed rather than a reduced value based on flanges only. This result is very important because contradicts the predictions from plastic theory, but it is confirmed by experimental tests. Moreover neglecting M-V interaction simplifies the analysis and design of shear links.

These results are very important because they permit to calculate the forces generated by the fully yield and strain hardened links. In fact, for links adjacent to columns, the ultimate link end moments can be taken as:

$$M_a = M_b = \frac{V_{ult} e}{2} \qquad \text{for } e \leq 1.3 \frac{M_p}{V_p} \tag{3.17}$$

$$M_a = M_p \;\; ; \;\; M_b = V_{ult} e - M_p \text{ for } 1.3 \frac{M_p}{V_p} \leq e \leq 1.6 \frac{M_p}{V_p} \tag{3.18}$$

where M_a and M_b are the link end moments at the column face and at the opposite end of the link. For links not adjacent to columns, the ultimate moments given by Equation 3.17 are appropriate for links of any length.

Several authors (such as Dusicka et al. 2004, Okazaki et al. 2004), observed during the experiments the locations of initial cracking in the web of steel built up shear links at stiffener to web interface (Figure 3.12a). Shear links that did not have stiffeners (Figure 3.12b) had lower plastic strain demands in the web as compared to those with stiffeners and consequently did not develop cracks until larger deformations were

imposed. Localized plastic strains were also present in the stiffeners and the flanges of the links. The stiffeners developed localized plastic hinging at the connection to the flange, resulting in the observed cracks during the experiments. The flange plastic strains developed near the ends of the effective length. Welding should be avoided in these locations in order to avoid potential for flange cracking, which may result in undesirable modes of failure (Figure 3.12c).

Fig. 3.12. Short link web fracture: location of initial crack in a stiffened link (Dusicka et al., 2004) (a); location of initial crack in an unstiffened link (Dusicka et al., 2004) (b); web fractures after testing for stiffened shear link (Okazaki et al. 2004) (c). (continued)

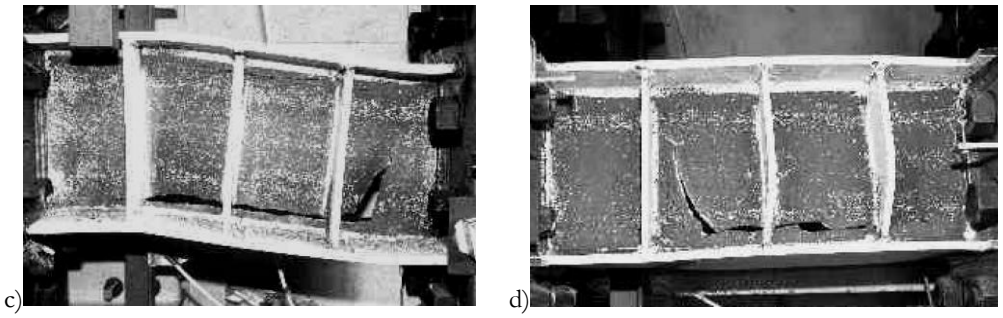

Figure 3.13. Short link web fracture: location of initial crack in a stiffened link (Dusicka et al., 2004) (a); location of initial crack in an unstiffened link (Dusicka et al., 2004) (b); web fractures after testing for stiffened shear link (Okazaki et al. 2004) (c,d).

Dusicka et al. (2004) developed detailed numerical models to investigate the plastic strain demands on the different components of the steel built up links (Fig. 3.14). A consistent correlation was found between the location of the initial cracking during the experiments on shear links with stiffeners and the location of localized plastic shear strain in the numerical models. The increase in strain demand occurred consistently at the ends of the stiffener to web connection, next to the stiffener chamfer. The plastic strains in those locations were over 20% higher than in the middle of the panel and coincided with the welding start and stop locations of the stiffener fillet welds.

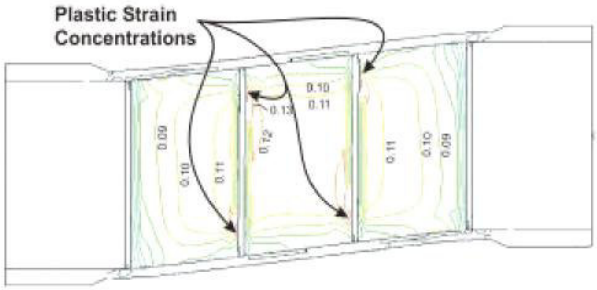

Fig. 3.14. Plastic strain distribution in web of built-up shear links (Dusicka et al., 2004).

This indicates that the onset of cracking in the web observed during the experiments was likely caused by the combination of the influence of the heat affected zone from welding and the plastic strain concentrations caused by the link deformations. No localized plastic strain concentrations occurred in the web in the link length. The contours of the plastic shear strain showed lower demand at the ends of the link length as compared to mid-length and overall showed less plastic strain demand. Besides, Dusicka et al. (2004) carried out an experimental and numerical study on built up links with low yield point steel. In this way the web thickness could be increased and stiffeners excluded. From the strain demand perspective, removing the stiffeners from the link length eliminated the localized plastic shear deformations caused by the presence of web stiffeners. As a result, the initial cracking and ultimate failure mode occurred at significantly higher link deformations for links that did not utilized stiffeners.

3.5 LINK ENERGY DISSIPATION

The ductile behaviour of EBs under severe seismic excitation relies on the capability of links to dissipate energy. For this reason, during the '70s and '80s, most of the experimental tests on steel links were carried out to quantify the energy dissipation capacity. Malley & Popov (1984) measured that the maximum ductility $\mu = \frac{\delta_{max}}{\delta_y}$ (where δ_{max} is the maximum relative link end displacement and δ_y is the relative link end displacement at yielding) varied from 31.9 to 66, while the cumulative ductility $\Sigma\mu$ (summation of μ for all cycles) from 237 to 751. The minimum values corresponded to unstiffened links, however all steel links manifested a significant energy dissipation capacity. Also, Kasai & Popov (1986a and 1986b) measured the link energy dissipation in their experimental activities. In particular, they measured:

1) E_e = elastic energy stored by the link at yield
2) E^* = the actual energy dissipated during each cycle

They verified that short links manifested larger values of E^* than longer links. Moreover they verified the existence of a constant relationship between E^*/E_e and a/t_w at the occurrence of web buckling.

As mentioned in the previous Sections, the main cause of energy absorption deterioration was the web buckling. In case of link with axial compressive force, the deterioration in energy was influenced by flanges buckling. In particular flange buckling more severely impaired the energy dissipation for the longer specimens than for the shorter ones.

Tests with an axial compressive force indicated the importance of preventing severe asymmetric local flange buckling in order to avoid premature failure. So an estimate of the flange yield zone length as it relates to the end moment is essential. Kasai & Popov (1986b) proposed a solution to define the shear link flange yield zone length. Their approach is summarized in Fig. 3.15, in which e_i is the distance between the end of a link and the inflection point, while ρ is the ratio between the axial force and the shear force acting in the link.

In particular, they assumed that the critical distance l_y from the end is sufficient to make the idealization that flanges resist the moment and the web the shear force. This idealization was confirmed by the experimental tests, which indicated that the portion of shear taken by the web rapidly

increased as the distance from the end increased. Hence, the yield zone length of flange in a shear link can be expressed as:

$$l_y = e_i\left(1 - \frac{M_p}{M_a}\right) + \rho\frac{M_p}{P_y} \qquad (3.19)$$

where the first term is the contribution of bending and the second from the axial force.

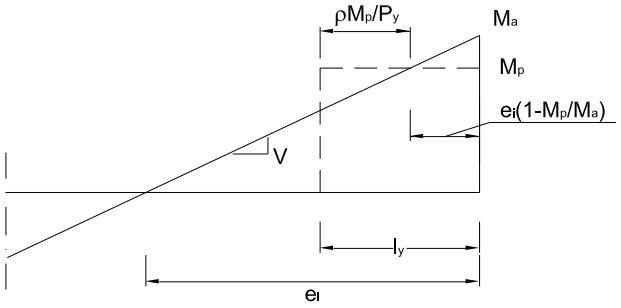

Fig. 3.15. Yield zone length of flange in a shear link (Kasai & Popov, 1986b).

3.6 LINK OVER-STRENGTH

One of the fundamental aspects characterizing the link behaviour is the over-strength factor defined as the ratio between the maximum shear force sustained by the element and the nominal shear yielding force (V_p). Link over-strength is primarily due to strain hardening, but it can also be due to the development of shear resistance in the link flanges. The link over-strength factor is used to estimate the maximum forces that can be generated by a fully yielded link, which in turn, is then used to design the non-dissipative elements as the diagonal braces, the beam segment outside of the link and the columns of the EBs. Past researchers have generally recommended a link over-strength factor of 1.5 (Popov and Engelhardt 1988). Recently, the 2002 AISC Seismic Provisions specified a link over-strength factor of 1.25 for design of the diagonal brace, and an over-strength factor of 1.1 for the design of the beam segment outside of the link and for the columns. As described in the Commentary of the 2002 AISC Seismic Provisions, because of AISC consider the average yield strength of material, capacity design rules in the provisions are based on an assumed over-strength factor. The over-

strength factor suggested by modern European design codes (Eurocode 8, 2003) is 1.5, a value basically coming from experimental results on American wide-flange shapes, carried out in the '80s (Kasai & Popov, 1986).

Test results demonstrate how the over-strength ratio varied significantly among the specimens and in most cases exceeded the expected values with a wide margin. In fact, recent tests on large built-up shear links for use in bridge applications and on European wide flange steel profiles showed over-strength factors greater than 1.5, reaching link over-strength of about 4 (Itani et al. 1998; McDaniel et al. 2003, Della Corte & Mazzolani 2005, Barecchia et al. 2006, D'Aniello et al. 2006).

Recently, in order to evaluate the consistency of this factor, numerous experimental tests have been carried out. Dusicka et al. (2004a) conducted some experimental tests and numerical studies on conventional and specialty steel for shear links and concluded that the over-strength factor ranges from 1.50 to 4.00. McDaniel et al. (2003) conducted cyclic tests on two full-scale built-up shear links for the main tower of the New San Francisco-Oakland Bay. The shear link over-strength factors were respectively 1.83 and 1.94.

The results of three experimental tests, carried out in the current research activity, showed values larger than 3.00 (Della Corte & Mazzolani 2006, D'Aniello et al. 2006). This has led to the concern that current over-strength factors may be unconservative, particularly for shapes with heavy flanges and in general for European wide flange hot rolled steel profiles (characterized by local slenderness ratio smaller than American ones), where shear resistance of the flanges can contribute significantly to over-strength. Moreover, these tests underlined the importance of the link boundary conditions. In fact, in case of end restraint conditions can be approximated as being fixed-fixed, It is contended that large deformations may produce an axial tension force whose effect is non-negligible. Tension axial forces are expected to increase ductility and peak inelastic shear strength.

Recently, Okazaki et al. (2004) conducted an experimental investigation to examine flange buckling and over-strength in links and this research program confirmed the importance of flange slenderness on rotational capacity and on the bearing capacity of short links, but the evidence of flange slenderness effects on link rotation capacity is still not clear. Moreover, the effect of link axial forces has been neglected.

3.7 LINK END-CONNECTIONS

Link end-connections represent a crucial aspect. In fact, in order to provide the reliable and effective dissipative behaviour, the link end-connections should be able to transfer the maximum link forces to the remaining parts of the structure without any sort of damages.
Generally speaking, some of the typical EBs are arranged to have one end of the link connected to a column and, in the last years, the main research efforts have been addressed to study these local details. In such EBs, the integrity of the link-to-column connection is fundamental in order to provide the ductile performance of the link, and therefore, the ductile performance and safety of the EBF.
Malley and Popov (1984) observed that the large cyclic shear force developed in EBF links could cause repetitive bolt slippage in welded flange-bolted web connections. The bolt slippage ultimately induced sudden failure of the connection by fracture near the link flange groove weld. Engelhardt and Popov (1992) tested long links attached to columns, and observed frequent failures at the link-to-column connections due to fracture of the link flange. Since these failures typically occurred before significant inelastic deformation was developed in the link, the authors recommended that EB arrangements with long links attached to columns should be avoided.
Besides the exceptions discussed above, the most of EB link-to-column connections have been designed and detailed very similar to beam-to-column connections in moment resisting frames. Therefore, many of the features responsible for the poor performance of moment connections during the 1994 Northridge earthquake are also present in link-to-column connections in EBs.
Recently an experimental and analytical investigation has been conducted by Okazaki et al. (2004) to study the performance of link-to-column connections in seismic resistant EBs. They tested link-to-column specimens with four different connection types and three different link lengths for each connection type, ranging from a short shear-yielding link to a long flexure-yielding link. These link-to-column specimens failed by fracture of the link flanges near the groove weld (Fig. 3.16). The Authors showed that the fracture typically developed rapidly, causing abrupt and severe degradation in the strength of the specimen. Moreover they report that link stiffeners provided an excellent buckling control by the left fracture at the link-to-column connection as the dominating

failure mode of the specimens. Another important aspect underlined by the authors is that the performance of the link-to-column connection depended strongly on the link length, with the inelastic link rotation capacity decreasing significantly with the increase in the link length. In fact the effects of the link length are reflected in the substantial difference in link shear force and column face moment. Test results suggest that premature failure of the link flange is a concern not only for connections of a long link to a column, but also for connections with short shear links.

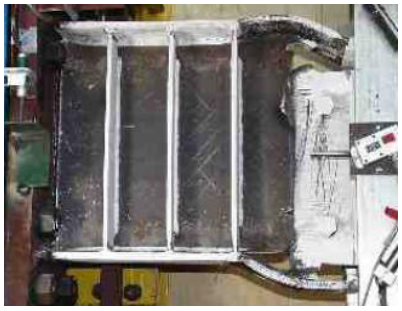

Fig. 3.16. Failure of link-to-column connection (Okazaki et al. 2004).

3.8 LINK MODELLING

Steel links are subjected to high levels of shear forces and bending moments in the active link regions. In the analysis of the performance of links, elastic and inelastic deformations of both the shear and flexural behaviours have to be taken into consideration. Few researchers attempted to develop link models for the dynamic inelastic analysis of EBs (Ricles & Popov 1994, Ramadan & Ghobarah 1995). Ramadan & Ghobarah modelled the link as a linear beam element with six nonlinear rotational and translational springs at each end. Three rotational bilinear springs were used to represent the flexural inelastic behaviour of the plastic hinge at the link end represented by the multilinear function shown in Fig. 3.17a. Three translational bilinear springs were used to represent the inelastic shear behaviour of the link web represented by the multilinear function shown in Fig. 3.17b.

Under the effect of cyclic loading, moment yielding obeys the kinematic hardening rule while shear yielding follows a combination of both

isotropic and kinematic hardening. For the shear spring, a special function was derived to account for the upper bound of the shear capacity (Ramadan & Ghobarah 1995). The function determines the maximum attainable shear force capacity after a certain amount of plastic action. This function has the following form:

$$V = V_p\left[1 + 0.8\left(1 - e^{-10S}\right)\right] \tag{3.20}$$

where V_p is the initial shear yield strength and S is the accumulated strain in the shear spring.

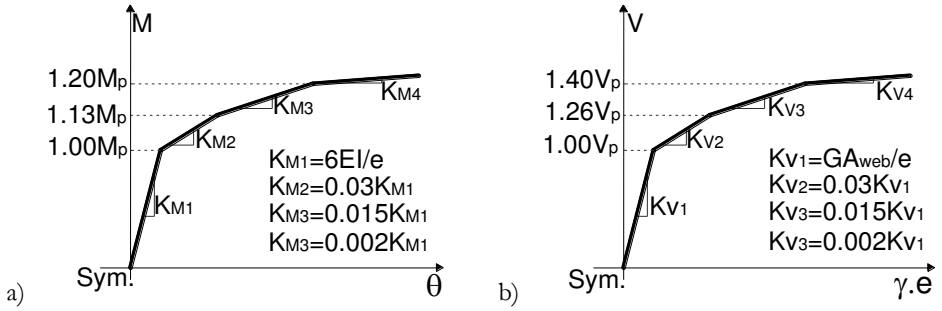

Fig. 3.17. Flexural inelastic behaviour of link plastic hinge (a); Shear inelastic behaviour of link plastic hinge (b).

3.9 DUAL ECCENTRIC BRACED FRAMES

Dual braced structures are constituted by eccentrically braced frames and moment resisting frames. A great number of works demonstrated that the seismic response of steel systems can benefit from the interaction between moment resisting frames (MRFs) and braced frames (Bosco et. al. 2013). Particulary, the interaction between between moment resisting frames and braced frames can reduce the interstorey displacements demanded by low intensity earthquakes to moment resisting frames (Martinelli et al. 1998) or the residual displacements developed by concentrically braced frames (Kiggins S et al. 2006). Other authors (Whittaker et al. 1998; Jain et al. 1993; Dubina et al. 2008; Khatib et al. 1998) have underlined that the presence of MRFs and braced frames in a single system can lessen the differences in the inelastic interstorey displacements along the height of the building and reduce the sensitivity

of the seismic response to realistic variations in the mechanical properties of members. Actually the design methods proposed by building codes for dual framed systems are simplistic and in many cases not very effective. In the earliest formal appearance of the dual framed system in codes, the MRF was conceived as a reserve system and designed to provide failsafe in the event of degradation of the braced frame (Hines et al. 2010). The codes which conceived as such the dual framed system required that the braced frames resisted the whole seismic load and that the MRFs were capable of resisting not less than 25 % of the design base shear. This design point of view has changed in the last years and recent codes testify the transition of the MRF from an independent reserve system to part of the primary lateral system. In accordance with this new view, braced frames and MRFs of dual systems are now designed to resist seismic forces which derive from the distribution of the seismic load between frames according to their lateral stiffness (EC8) and to control the strength and stiffness of the MRFs, some building codes (AISC 341 and ASCE 7-05) also require that the MRFs are designed to resist at least 25% of the design base shear. These design provisions do not ensure a substantial improvement in the seismic behaviour of braced structures because often the lateral strength and particularly the stiffness of the MRFs are much lower than those of the braced frames. Whittaker et al. proposed designing MRFs for a higher lateral stiffness and strength. The design method remained centred on provisions which referred to global structural properties but it was not able to adjust the lateral stiffness and strength of the single storey so as to achieve assigned distributions of the interstorey displacements. Also, the design method did not consider the deformative capacity of the single storey and thus was not able to ensure fairly uniform distributions of damage in the elements designated to the inelastic response.

REFERENCES

- Roeder C.W., Popov E.P., (1978). Eccentrically Braced Steel Frames for Earthquakes, Journal of Structural Engineering, American Society of Civil Engineers, Volume 104, Number 3.
- Kasai K., Popov E.P,. (1986a). General Behavior of WF Steel Shear Link Beams. Journal of Structural Engineering, vol.112, No. 2, 362-382, 1986
- Kasai K., Popov E.P., (1986b). Cyclic Web Buckling Control for Shear Link Beams. Journal of Structural Engineering, vol.112, No. 3, 505-523.
- Popov E.P., Malley J.O., (1983) Design of links and beam-to-column connections for eccentrically braced steel frames. Report No. EERC 83-03.
- Hjelmstad K.D., Popov E.P., (1983). Cyclic Behavior and Design of Link Beams. Journal of Structural Engineering, vol.109, No. 10, 2387-2403,.
- Ricles J.M., Popov E.P. (1987). Dynamic analysis of seismically resistant eccentrically braced frames. Earthquake Engineering Research Center, University of California, Berkeley.
- Engelhardt M.D, Popov E.P,, (1989). On Design of Eccentrically Braced Frames. Earthquake Spectra, vol.5, No.3, 495-511.
- Itani A, Douglas B.M. & ElFass S., (1998). Cyclic behavior of shear links in retrofitted Richmond-SanRafael Bridge towers. Proceedings of the First World Congress on Structural Engineering – San Francisco, Paper No. T155-3, Elsevier Science Ltd.
- Nader M., Lopez-Jara J. & Mibelli, C., (2002). Seismic Design Strategy of the New San Francisco-Oakland Bay Bridge Self-Anchored Suspension Span, Proceedings of the Third National Seismic Conference & Workshop on Bridges & Highways, MCEER Publications, State University of New York, Buffalo, NY.

- Foutch D.A., (1989). Seismic Behavior of Eccentrically Braced Steel Building. Journal of Structural Engineering, vol.115, No. 8, 1857-1876.
- Gerard, G., (1948). Critical Shear Stress of Plates above the Proportional Limit. Journal of Applied Mechanics Engineering, vol.15, No. 1, 7-12
- Dusicka P., Itani A. M. & Buckle I. G., (2004a). Evaluation of Conventional and Speciality Steels in Shear Link Hysteretic Energy Dissipators. Proceedings of the 13th World Conference on Earthquake Engineering, (CD-ROM, paper n. 522), Vancouver, Canada.
- Okakazi T., Arce G., Ryu H., Engelhardt M.D., (2004). Recent Research on Link Performance in Steel Eccentrically Braced Frames, Proceedings of the 13th World Conference on Earthquake Engineering, B.C. Canada.
- Malley J.O., Popov E.P., (1984). Shear Links in Eccentrically Braced Frames. Journal of Structural Engineering, vol.110, No. 9, 2275-2295.
- Mc Daniel, C. C., Uang, C. & Seible, F., (2003). Cyclic Testing of Built-Up Steel Shear Links for the new Bay Bridge. Journal of Structural Engineering, vol. 129, No 6.
- Della Corte G., D'Aniello M., Mazzolani F.M., (2005). "Seismic Upgrading of RC buildings using Buckling Restrained Braces: full-scale experimental tests". XX C.T.A. Conference – First Int. Workshop on ADVANCES IN STEEL CONSTRUCTIONS, Ischia (Italy), 26-28 September.
- Barecchia E., Della Corte G., Mazzolani F..M., (2006). Plastic over-strength of short and intermediate links. Proceedings of the STESSA Conference, Yokohama, Japan.
- D'Aniello M., Della Corte G., Mazzolani F.M, (2006). "Design Methods for Eccentric Braces". WP9 data sheet of PROHITECH project.

- Dusicka P., Itani A. M. & Buckle I. G., (2004a). Evaluation of Conventional and Speciality Steels in Shear Link Hysteretic Energy Dissipators. Proceedings of the 13th World Conference on Earthquake Engineering, (CD-ROM, paper n. 522), Vancouver, Canada.
- Okakazi T., Arce G., Ryu H., Engelhardt M.D., (2004). Recent Research on Link Performance in Steel Eccentrically Braced Frames, Proceedings of the 13th World Conference on Earthquake Engineering, B.C. Canada.
- Okazaki T., Engelhardt M.D. (2007). Cyclic loading behavior of EBF links constructed of ASTM A992 steel. Journal of constructional Steel Research, 63, 751-765.
- Ramadan T, Ghobarah A., (1995). Analytical model for shear–link behavior. J Struct Engng, ASCE, 121(11):1574–80.
- M. Bosco, P.P. Rossi (2013). A design procedure for dual eccentrically braced systems: Numerical investigation. Journal of constructional Steel Research, 80: 453–464
- Martinelli L, Mulas MG, Perotti F. (1998). The seismic behaviour of steel moment-resisting frames with stiffnening braces. Eng Struct;20(12):1045-62.
- Kiggins S, Uang C. 2006. Reducing residual drift of buckling-restrained braced frames as a dual system. Eng Struct;28:1525-32.
- Whittaker AS, Uang C, Bertero VV. 1998. An experimental study of the behaviour of dual steel systems. Earthquake Engineering Research Center, Report No. UCB/EERC-88/14. University of California.
- Jain AK, Redwood RG, Lu F. 1993. Seismic response of concentrically braced dual steel frames. Can J Civ Eng;20:672-87.
- Dubina D, Stratan A, Muntean N, Dinu F. 2008. Experimental programfor evaluation of moment beam-to column joints of high-strength steel components. Sixth International Workshop

on Connections in Steel Structures. American Institute of Steel Construction.

- Khatib IF, Mahin SA, Pister KS. 1998. Seismic behaviour of concentrically braced steel frames. Earthquake Engineering Research Center, Report No. UCB/EERC-88/01. University of California.
- Hines EM, Fahnestock LA. Design philosophy for steel structures inmoderate seismic regions. 9th US National and 10th Canadian Conference on Earthquake Engineering, EERI/CAEE, Toronto, Canada; July 2010.
- Eurocode 8. 2003. Design of structures for earthquake resistance. Part 1: general rules, seismic actions and rules for buildings. European Committee for Standardisation. prEN 1998-1-1/2/3.
- AISC 341-05-AISC 341s1-05. 2005. Seismic Provisions for Structural Steel Buildings incl. Supplement No. 1. American Institute of Steel Construction, Inc.
- ASCE 7–05. 2006. Minimum design loads for buildings and other structures incl. Supplement No.1. American Society of Civil Engineers0-7844-083-1-9.

4 PARAMETRIC ANALYSIS

4.1 INTRODUCTION

A total number of thirty-two EBFs and D-EBFs were designed in accordance with EN1998-1 using S460 and S690 (HSS) for columns and S355 (MCS) for beams. The investigated parameters were the following:

- number of storeys: eight-storey and sixteen-storey frames, as shown in fig. 4.1, where the height of first floor is 4.0 m and all other are 3.5 m;
- span length : 5.0 m and 7.5 m;
- composite steel-concrete column typologies: fully encased (FE), partially encased (PE);
- corner period of the design spectra: two types of soil conditions have been examined. The former representative of soil type C according to EN1998-1 (hereinafter identified as "stiff soil") and the latter representative of very soft soil conditions with corner period of 1.6 s, which are representative of specific soil condition in Bucarest (hereinafter identified as "soft soil");

In order to identify each structure, a label code has been given to the frames as follows:
EBF or DEBF_(stories).(steel).(Span).(Soil).(Column)
where:
(stories) = 1 for eight-stories and = 2 for sixteen-stories;
(steel non dissipative members) = 1 S460 = 2 S690;
(Span) = 1 for 5.0 meters span and = 2 for 7.5 meters span;
(Soil) = 1 for stiff soil and = 2 for soft soil;
(Column) = 1 for fully encased columns, = 2 for partially encased.

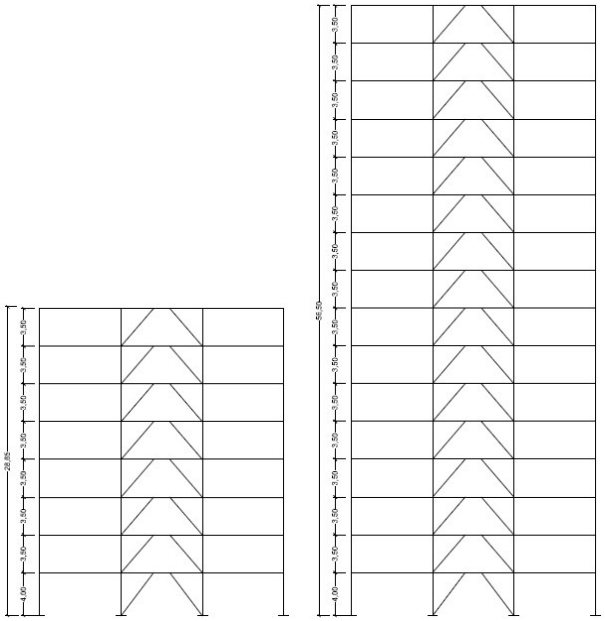

eight-storey **sixteen-storey**

Fig. 4.1 Structural scheme of study cases

The frames integrate the structural system of buildings (fig. 4.2) that comply with the regularity conditions in plan and elevations, according to EN1998-1. Floors consist of orthogonal steel beams (primary and secondary) and steel-concrete composite columns. Primary beams are considered braced to avoid lateral-torsional buckling in order to allow for plastic deformation in bending. All beam-column joints were assumed as full strength and full rigid. The columns were considered to be fixed at the base and continuous through the height. In plan, columns are spaced at L = 7.5 m or L = 5.0 m in both directions, as depicted in fig. 4.2

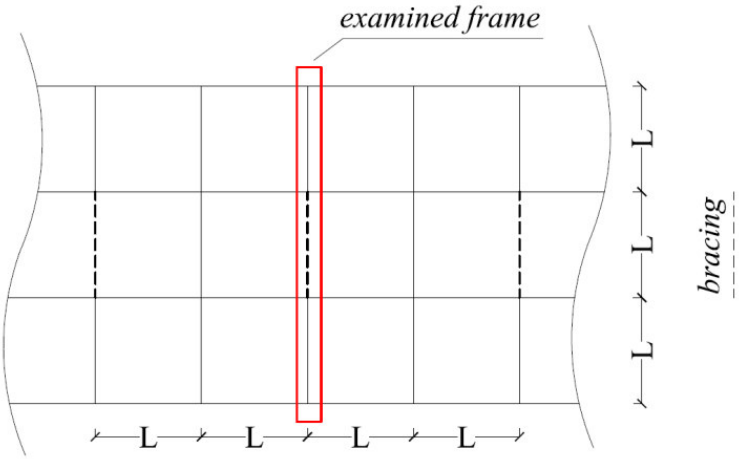

Fig.4.2 Structural scheme of study cases

4.2 PERFORMANCE LEVELS

The seismic hazard curve provided by EN1998-3 is defined with the following equation:

$$H\left(a_{gR}\right)=k_o\left(a_{gR}\right)^{-k} \qquad (4.1)$$

where a_{gR} is the reference peak ground acceleration, while the exponent k depends on seismicity, but being generally assumed equal to 3.

The seismic performance of study cases is evaluated for three performance levels, which are associated to different annual rate of exceedance: damage limitation (DL), severe damage (SD) and near collapse (NC).

According to EN1998-3 at the DL state the building is subjected to the frequent earthquake with 95-year-return period, the structure shall have no occurrence of damage and the associated limitations of use. EN1998-3 presented a reduction factor ν to take into account the determination of the frequent earthquake from the design earthquake. In the examined cases ν is equal to 0.5 and the corresponding structural performance should provide interstorey drift ratios lesser than 0.75%.

The SD state corresponds to design condition where the structure shall have no local or global collapse under the design seismic action with 475-year-return period. At this performance level, the structure is strongly damaged but has some residual lateral strength and stiffness and vertical elements are capable of sustaining vertical loads, thus providing

the strength to sustain moderate after-shocks. To verify the effectiveness of the structural performance, a limit value for residual drift equal to 0.4% has been assumed.
At the NC state the structures are expected to be heavily damaged, with negligible residual lateral strength and stiffness, although vertical elements are still capable of sustaining vertical loads. Large permanent drifts are present. The structures are near collapse and are not able to resist to moderate earthquake after-shocks. In this study is assumed to verify this performance level against a seismic action with 2475-year-return period. An interstorey drift of 3.0% has been assumed to characterize this damage scenario as early proposed by Grecea et. al. (2004).□
Table 4.1 summarizes the performance levels used for each of the three limit states where acceleration ratio Ad corresponds to peak ground acceleration used in design.

Table 4.1: Performance levels

Limit state	Return period (years)	A/A_d	Failure criteria
Damage limitation (DL)	95	0.59	0.75% interstorey drift ratio
Severe damage (SD)	475	1.00	0.40% residual interstorey drift ratio
Near collapse (NC)	2475	1.72	3.0% interstorey drift ratio

4.3 SEISMIC DESIGN

The frames were designed in accordance with EN1998-1, EN1993-1 and EN1994-1. In the design calculations, first order elastic analyses have been carried out with amplification of relevant action effects to account for P-Delta effects. In addition, the effects of initial sway imperfection have been taken into account by systems of equivalent horizontal forces as indicated by EN1993:1-1.
As damage limitation requirement, the maximum interstorey drift was fixed equal to 0.75%, thus assuming ductile non-structural elements.
Dead and live loads equal to 4.0 kN/m^2 and 3.0 kN/m^2, respectively, were considered. The peak ground acceleration was assumed as 0.32 g for stiff and soft soil too. The reference behaviour factor was assumed to

be q = 6.0. Fig. 4.3 shows the both elastic and design spectra for the frames located on stiff or soft soil.

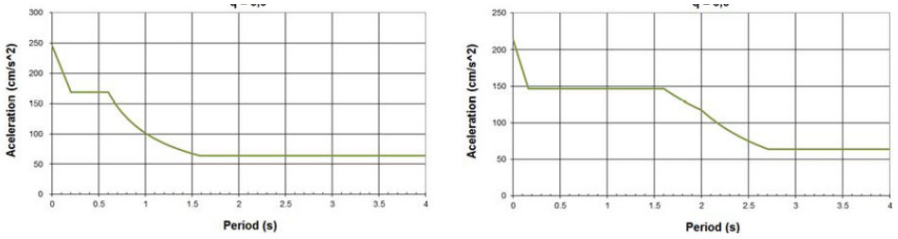

a) **b)**

Fig.4.3 Design spectra for stiff (a) and soft soil (b)

The design forces have been calculated by means of standard modal response spectrum analyses, according to EN1998-1, where all modes of vibration that contribute significantly to the global response were taken into account. The designed cross sections for beam and columns and the relevant first and second natural periods per structure are reported in the annex 1.

4.4 NUMERICAL MODELS

In order to assess the seismic behaviour of frames both nonlinear static and dynamic analyses have been performed using the software SeismoStruct.

The models were developed using the force-based (FB) distributed inelasticity elements (Spacone et al. 1996 – Calabrese et al. 2010). These elements account for distributed inelasticity through integration of material response over the cross section and integration of the section response along the length of the element. The cross-section behaviour is reproduced by means of the fibre approach, assigning a uniaxial stress-strain relationship at each fibre.

The stress-strain relationship for concrete fibres in the column elements was determined using the model proposed by Martinez-Rueda and Elnashai (1997). The effects of confinement provided by steel profile and/or reinforcement has been determined according to Mander et al. (1998) and Susantha et al. (2001), for fully/partially encased and concrete filled tube, respectively.

In the case of steel members, the model proposed by Menegotto and Pinto (1973) for the stress-strain curve was chosen.

The average values of both concrete compression strength and steel yield stress have been used. The former has been assumed according to EN 1992:1-1, while different values of material overstrength factor (γ_{ov}) for each steel grade. In particular, γ_{ov} equal to 1.25 was assumed for S355, while 1.10 for S460 (RFSR-CT-2007-00039).
The numerical integration method used is based on the Gauss-Lobatto distribution (Abramowitz et al. 1964), which includes, at a minimum, monitoring points at each end of the element. Such feature allows each structural member to be modelled with a single FE element, thus requiring no meshing for each element. In the present study, five Gauss-Lobatto integration points have been used.
Second order effects have been accounted in all analyses presented in this paper, by assuming large displacements/rotations.
The validity of the modelling assumptions has been verified against the experimental results carried out by D'Aniello et al. (2012) on steel beams. The comparison between experimental and numerical response curves are depicted in Fig. 4.4 , where it can be noted the satisfactory accuracy of the implemented numerical models.

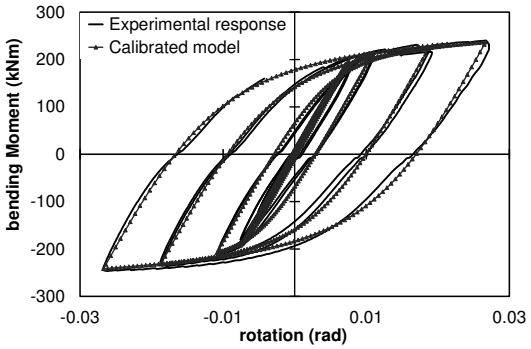

Fig. 4.4. Comparison between numerical and experimental curves: cyclic tests on steel beams by D'Aniello et al.

Concerning dynamic analyses a 2% Rayleigh tangent stiffness damping has been used at both first and second mode.
The braces were modelled with two elements only, arranged to have a bilinear shape with an initial camber (Δ_0). Figure 4.5 schematically shows the type of model adopted in this study, where integration points (IP) and the end joints (Ji) are clearly highlighted.

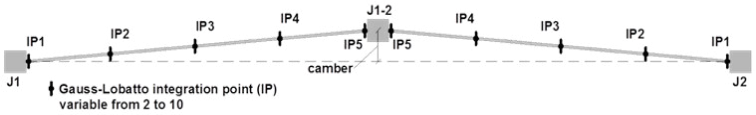

Figure 4.5. The implemented model to mimic the brace behaviour.

An initial camber is introduced to account for buckling of braces. In particular, Dicleli & Calik model is used, according the results of D'Aniello et al. (2013). The initial camber Δ_0 is derived assuming that the sinusoidal deformed shape of the brace prior to buckling and the imposing the second order flexural equilibrium in the section located at the mid-length of the buckling semi-wave, Δ_0 is obtained as follows:

$$\Delta_0 = \frac{M_{pb}}{N_b\left(1+\frac{N_b L^2}{8EI\left(1-\frac{N_b L^2}{\pi^2 EI}\right)}\right)} \quad (4.1)$$

Links are modelled by means of an inelastic fibre element and by a bi-linear kinematic spring at both ends. The central element has the same length and inertia as the link and simulates the flexural behaviour of links (the shear stiffness of this element is set to zero). The two ending springs are zero-length. They connect the beam segments outside the link to the flexural element of the link and reproduce the shear behaviour of the link. Only relative vertical displacements are permitted between the nodes of the shear element. The stiffness of the translational spring which causes this relative movement is defined to simulate the effect of the shear deformability of half a link. Short links are considered. The ultimate link shear force and bending moment are given by:

$V_u = 1.5V_p$ (4.2)

$M_u = 0.5eV_u$ (4.3)

Being e the link length.

The post-yielding stiffness of the shear springs is defined as follows:

$$K_v = \frac{0.5V_p}{0.08} \quad 4.4$$

Being 0.08 the maximum plastic rotation in radians

Accuracy of modelling assumptions was verified by comparison of theoretical outcomes with experimental results obtained by Okazaki and

Engelhardt (2007). The examined link is made of an US wide flange hot-rolled profile W10x33, having

$$\frac{e \cdot V_p}{M_p} = 1.04 \qquad (4.5)$$

In Figure 4.6 it is depicted the comparison between experimental and numerical response of the examined link. As it can be observed the model matches very well the experimental response.

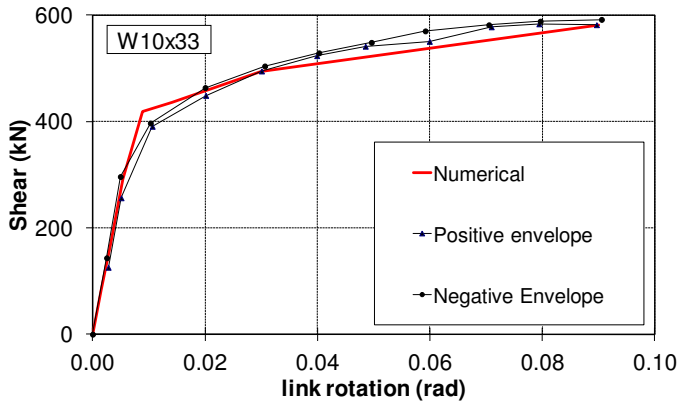

Fig 4.6. Link model vs. experimental response (Okazaki and Engelhardt, 2007).

4.5 NONLINEAR ANALYSES - PUSHOVER

The pushover analyses were carried out applying two types of lateral load distribution, the first proportional to the first mode and the second a uniform distribution along frame height.

The response parameters monitored by the performed pushover analyses are illustrated in fig. 4.7. In particular, V_y refers to the yield strength of the structure, V_{1y} is the base shear at the formation of the first plastic hinge and V_d corresponds to the design base shear; δ_{1y} and δ_{max} are displacements corresponding to the formation of the first plastic hinge and ultimate displacement, respectively.

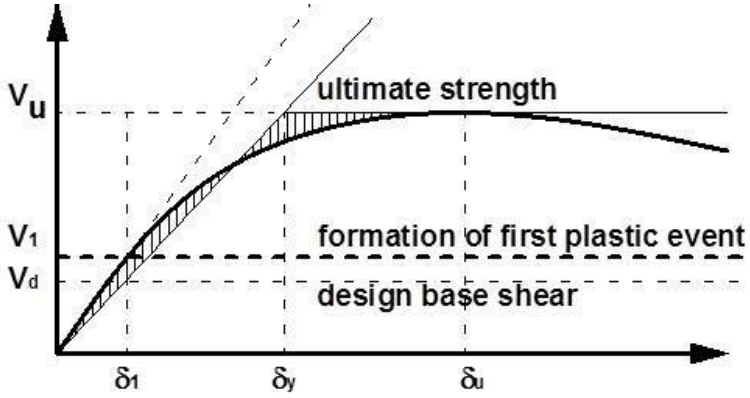

Fig. 4.7. Parameters monitored in pushover analyses.

4.6 OVERALL OVERSTRENGTH FACTOR

The overall overstrength factor Ω is defined as the ratio between the base shear corresponding to the overall yield strength of the frame and the design base shear. This ratio can be decomposed in two terms:

$$\Omega = \frac{V_y}{V_d} = \frac{V_y}{V_{1y}} \times \frac{V_{1y}}{V_d} \qquad (4.6)$$

where the first term, V_y/V_{1y}, corresponds to α_u/α_1 defined in the EN1998-1. This value depends on the frame configuration, formation of the collapse mechanism, redistribution capacity and gravity loading (Elghazoulli 2005). The second term (V_{1y}/V_d) is related to aspects of the design procedure such as differences between actual and nominal material strength, member oversizing due to choices of commercial cross-section and design governed by deformation and/or non-seismic loading.

Table 4.2 reports the V_1/V_d ratios obtained from the pushover analyses of the frames, while in the fig. 4.8 is depicted the related diagram.

Then, table 4.3 reports the V_u/V_1 factors obtained from the pushover analyses of the frames, while in the fig. 4.9 is depicted the related diagram.

Table 4.2: V_1/V_d ratios

	8-Storey				16-Storey			
	Stiff Soil		Soft Soil		Stiff Soil		Soft Soil	
	EBF	D-EBF	EBF	D-EBF	EBF	D-EBF	EBF	D-EBF
Average	2.61	2.91	1.92	2.46	3.02	4.64	2.28	3.84
Standard Deviation	0.26	0.40	0.23	0.11	0.06	0.27	0.45	0.03

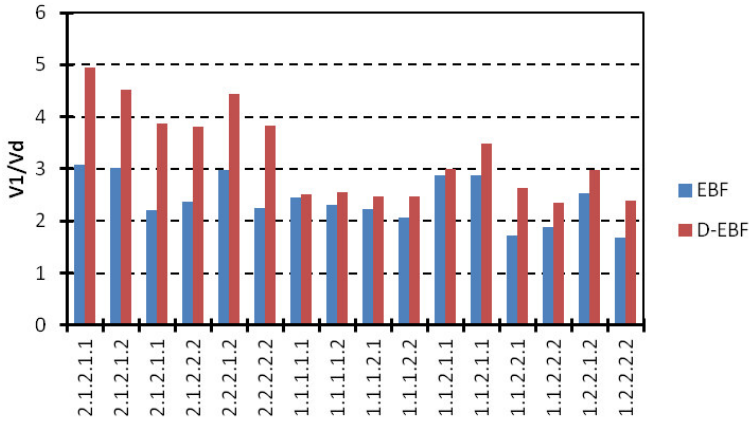

Fig. 4.8. V_1/V_d ratios

It's important to note that the D-EBFs presented higher design overstrength factors than the EBFs, this is due to the design assumption (plastic design), then there is a increasing of factor when the number of storey is increased.

Table 4.3: V_u/V_1 ratios

	8-Storey				16-Storey			
	Stiff Soil		Soft Soil		Stiff Soil		Soft Soil	
	EBF	DEBF	EBF	DEBF	EBF	DEBF	EBF	DEBF
Average	1.26	1.49	1.35	1.48	1.52	1.41	1.54	1.41
Standard Deviation	0.07	0.08	0.13	0.06	0.02	0.06	0.02	0.07

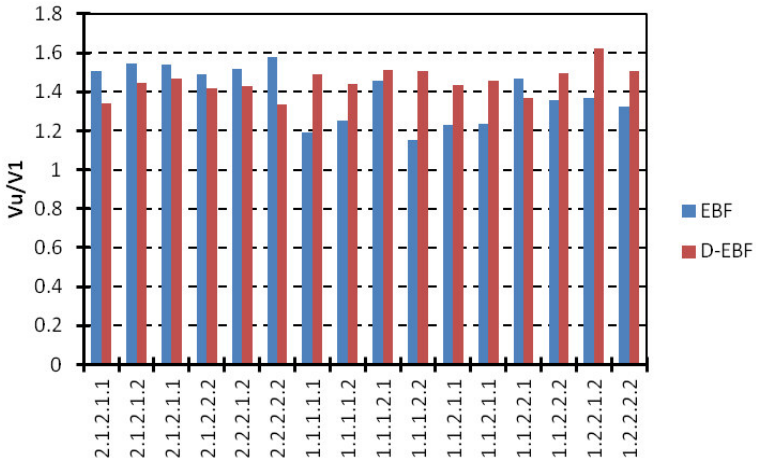

Fig. 4.9. V_u/V_1 ratios

For what concern the V_u/V_1 the D-EBFs presented higher factors ($\alpha u/\alpha 1$) than the EBFs for 8-storey while this trend is inverted for 16-storey

4.7 INCREMENTAL DYNAMIC ANALYSES

Two sets of both artificial and natural accelerograms have been used to perform nonlinear dynamic analyses. These records have been selected to match the elastic spectra given by EN1998-1 according to the procedure described in Fulop 2010. Figure 4.10 depicts the comparison between the codified response spectra and those given by each record and the relevant mean spectrum.

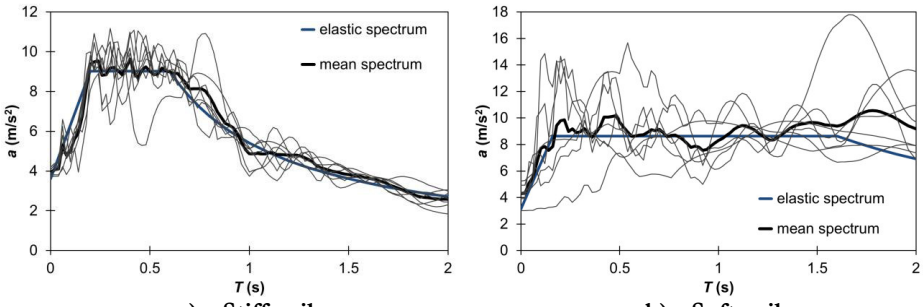

a) Stiff soil **b) Soft soil**

Fig. 4.10 Response spectra of selected accelerograms vs. EC8 response spectra.

Incremental dynamic analyses (IDAs) were carried out scaling the PGA up to 8 times the design value, as follows:
from 0.5 PGA to 8 PGA with a scaling step of 0.5.
Nonlinear incremental dynamic analyses were performed to characterize both the inelastic behaviour and the performance against the three reference limit states defined by EN1998-3. Fig. 4.11 and 4.12 depict the capacity curves from incremental dynamic analyses giving focus to type of soil and structural system, rather EBFs and DEBFs. These curves correspond to relation between the base shear normalized (base shear divided by design base shear) with the maximum roof displacement. As what is observed for pushover analyses, the curves show that the structures located on stiff soil have larger V/V_d ratios in comparison with than those located on soft soil; this trend is confirmed for EBFs and DEBFs too.

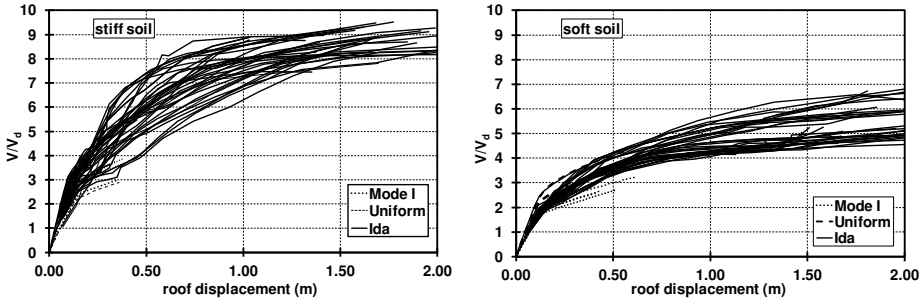

a)stiff soil **b)soft soil**

Fig. 4.11 Idas and Pushover for EBFs

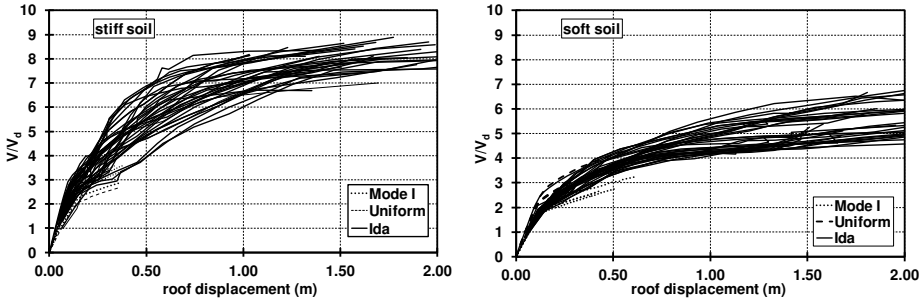

a)stiff soil **b)soft soil**

Fig. 4.12 Idas and Pushover for DEBFs

4.8 BEHAVIOUR FACTORS

In the EN1998-1, the behaviour factor of steel structures is defined as follows:

$$q = \alpha \times \frac{A_u}{A_y} \tag{4.7}$$

where A_u is the peak ground acceleration leading to accepted failure for the selected performance level, A_y is the peak ground acceleration corresponding to the yielding of the frame and α is the overstrength factor from pushover analysis allowing for different geometries of the frames.

In the present study the values of A_y and A_u have been derived from IDAs. The amplitude corresponding to the acceleration Au is the minimum value corresponding to all possible theoretical states of collapse:

$$A_u = \min(A_\theta, A_c, A_L, A_B) \tag{4.8}$$

where A_θ is the acceleration corresponding to the maximum permitted inter-story drift ratio;

A_c corresponds to the column or brace buckling;

A_L corresponds to the maximum permitted link rotation (as given by EN1998-3);

A_B corresponds to the maximum permitted beam rotation (DEBFs)

Fig. 4.13 shows the behaviour factors obtained and table 4.4 and 4.5 the median behaviour factors obtained and the 16th and 84th percentiles for SD and NC limit state. The behaviour factors obtained for both limite state are obviously smaller than design behaviour factors.

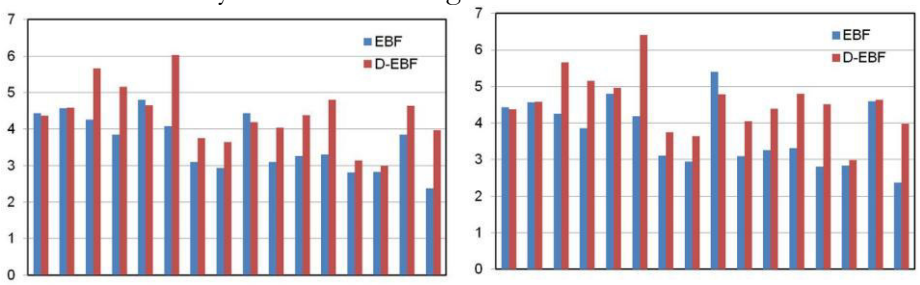

a)SD **b)NC**

Fig. 4.13 Behaviour factors

Table 4.4: Behaviour factors - SD

SD	8-Storey				16-Storey			
	Stiff Soil		Soft Soil		Stiff Soil		Soft Soil	
	EBF	DEBF	EBF	DEBF	EBF	DEBF	EBF	DEBF
16th	3.05	3.71	2.82	3.09	4.48	4.44	3.93	4.41
50th	**3.26**	**4.39**	**3.10**	**3.98**	**4.57**	**4.59**	**4.08**	**4.94**
84th	3.50	4.70	4.06	4.10	4.73	4.64	4.20	6.19

Table 4.5: Behaviour factors - NC

NC	8-Storey				16-Storey			
	Stiff Soil		Soft Soil		Stiff Soil		Soft Soil	
	EBF	DEBF	EBF	DEBF	EBF	DEBF	EBF	DEBF
16th	3.05	3.71	2.82	3.62	4.48	4.44	3.96	5.32
50th	**3.26**	**4.39**	**3.10**	**4.05**	**4.57**	**4.59**	**4.18**	**5.67**
84th	3.77	4.70	4.89	4.61	4.73	4.84	4.23	6.17

The performance of most of frames (both EBFs and D-EBFs) was affected by brace buckling, which occurred before the achievement of link rotation capacity. To improve the seismic performance the set of frames was redesigned using the maximum over-strength ratios $\Omega i = 1.5V_{pl,Rd,i}/V_{Ed,I}$ to design the braces only. In most of cases, it was possible to achieve this goal by simply scaling the steel grade for braces; hence, the same cross section but using S490 or S690 for braces.
The results in fig. 4.14 show a larger increase of q factor, sligthly larger than EC8.

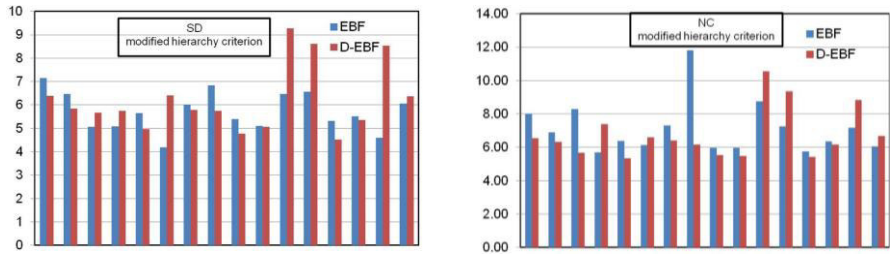

a)SD **b)NC**

Fig. 4.14 Behaviour factors – modified hierarchy criterion

4.9 PERFORMANCE EVALUATION

The performance indicators monitored for all limit states are the following: i) peak interstorey drift ratios; ii) residual interstorey drift ratios; iii) peak storey accelerations. The results are presented hereinafter.

4.9.1 Peak interstorey drift ratios

Errore. L'origine riferimento non è stata trovata. Fig. 4.15-4.16-4.17 depicts the interstorey drift ratio (IDR) demand along the height for the three limit states. As a general remark, the examined design parameters do not highlight appreciable influence on the IDR demand. The IDR demand at each limit state was fairly lower than the performance limits, substantially EBF and DEBF systems don't show problems related to interstorey drift ratio. The median values of IDR at DL state are lower than the limit of 0.75%. At DL state all frames behave in elastic field. The median IDR for the SD also in the range 1% - 1.5% while for the NC the IDR is in the range 1.5% - 2.0%

EBFs **DEBFs**

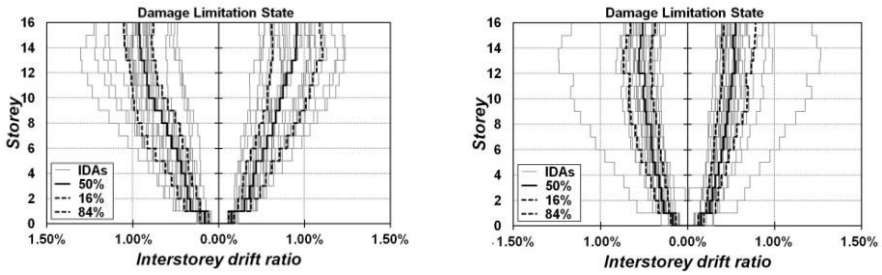

16-storeys

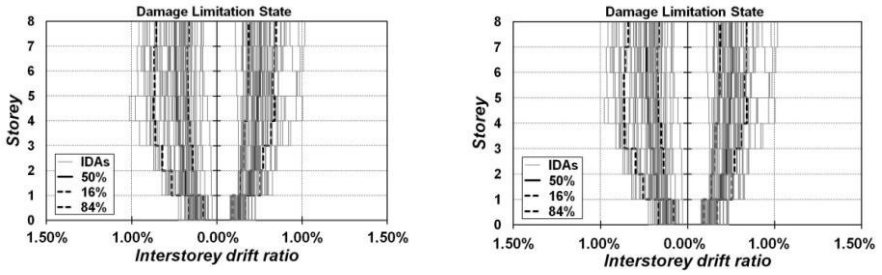

8-storeys

Fig. 4.15. Interstorey drift ratio - DL

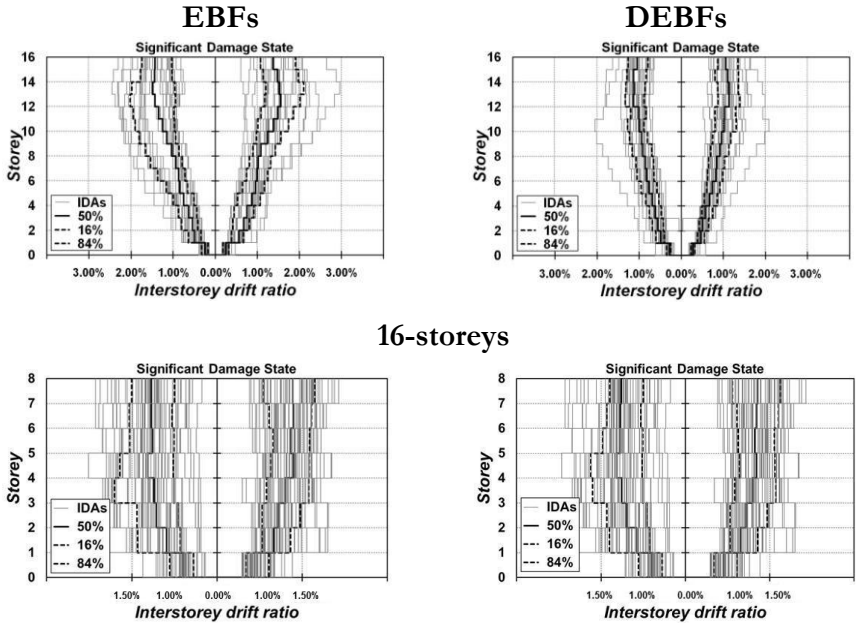

Fig. 4.16. Interstorey drift ratio - SD

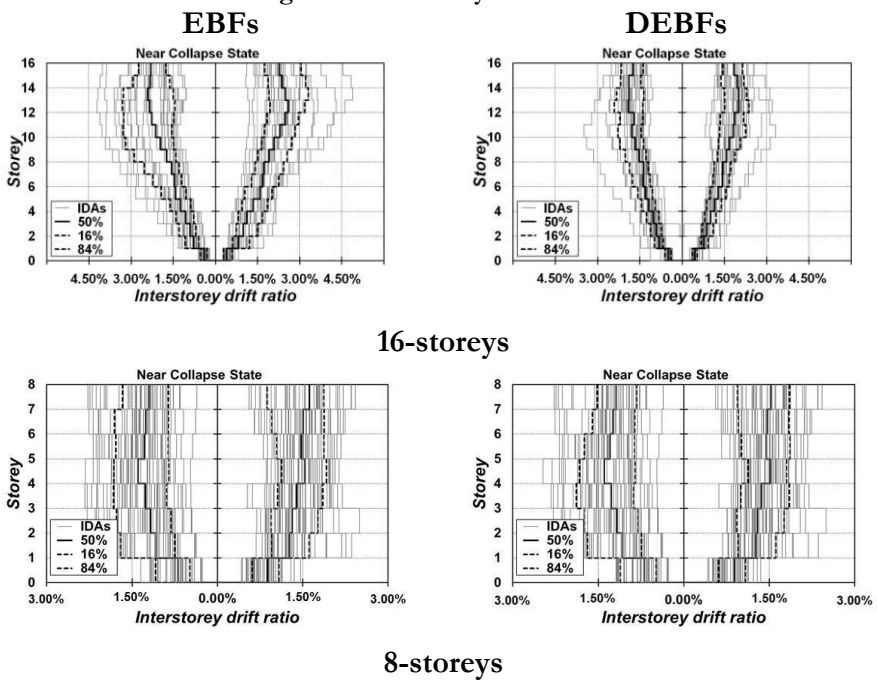

Fig. 4.17. Interstorey drift ratio - NC

4.9.2 Residual interstorey drift ratios

The residual interstorey drift ratios (RIDR) have been monitored at each limit state, because they provide useful data on the damage distribution and on the post-quake reparability of the frames.

As discussed in the previous section, at DL state all frames behave elastically and no linear events were observed, except for some cracking in the composite columns. Hence, the RIDRs are closed to zero at this limit state.

Only at SD and NC limit states the RIDRs have been recognized, and the median values and their percentiles are depicted in Fig. 4.18 – 4.19. It can be noted that the maximum values are lower than the limit of 0.40%. In particular, the maximum median RIDRs are equal to about 0.05% and 0.1% at SD and NC limit state, respectively. Concerning the design parameters, those most influential on RIDRs are the number of storeys and the soil condition. Indeed, all 16-storey frames showed residual drift larger than 8-storey frames. Regarding the soil conditions, the larger RIDRs were observed in frames designed for stiff soil, namely, a value of

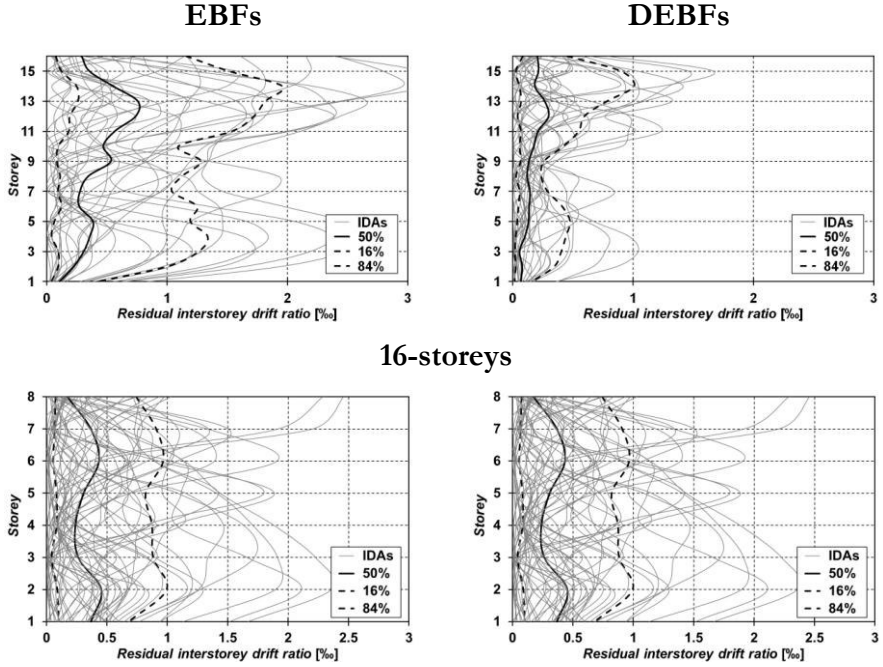

8-storeys

Fig. 4.18. Residual Interstorey drift ratio - SD

EBFs **DEBFs**

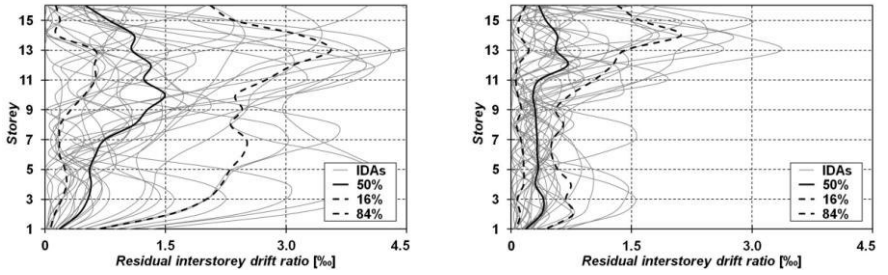

16-storeys

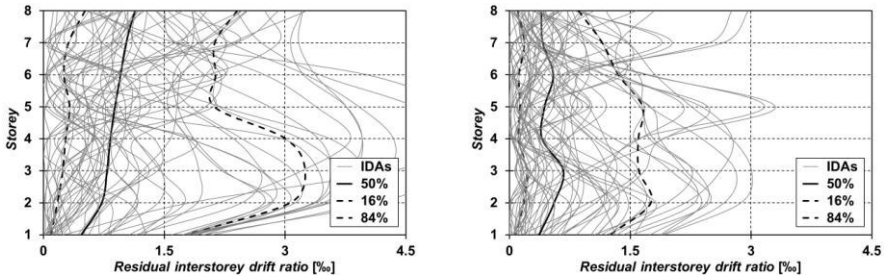

8-storeys

Fig. 4.19. Residual Interstorey drift ratio - NC

4.9.3 Peak storey accelerations

Peak storey accelerations (PSAs) are usually related to the non-structural damage, thus allowing to quantify the potential economic loss depending on the type of facilities and non-structural elements. Fig. 4.20 – 4.21 – 4.22 show the distribution of the median values of PSA along the building height for each limit state and their percentiles. The results are shown varying the number of storeys and the soil conditions. It is interesting to note that the median maxima PSA are similar for both 8- and 16-storey buildings, On what concern to maximum values, these scatters are verified on the upper storey. This may be ascribable to the higher modes in nonlinear conditions. The medium values of PSAs is equal to 0.2g at damage limitation state, and 0.3g and 0.5 g at SD and NC limit state, respectively

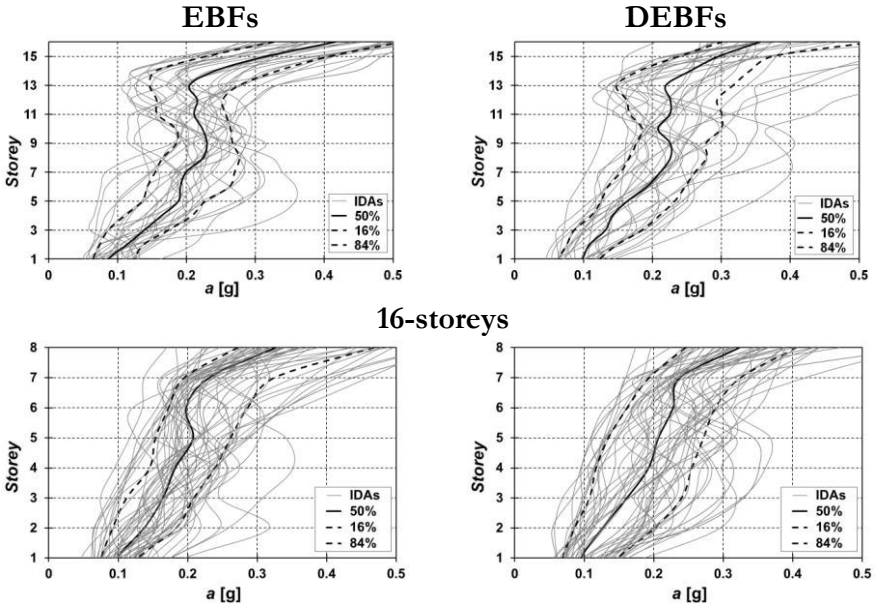

Fig. 4.20. Peak storey accelerations - DL

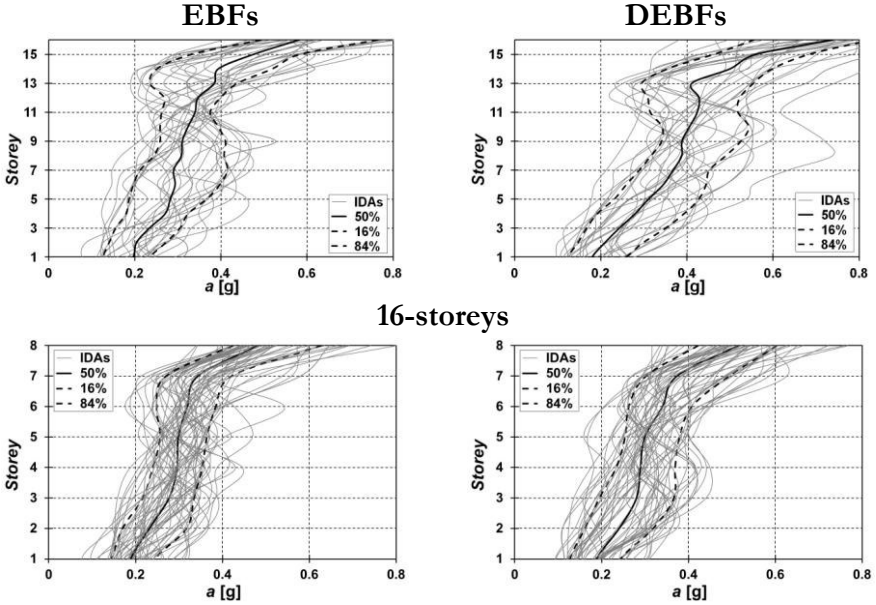

8-storeys

Fig. 4.21. Peak storey accelerations - SD

EBFs **DEBFs**

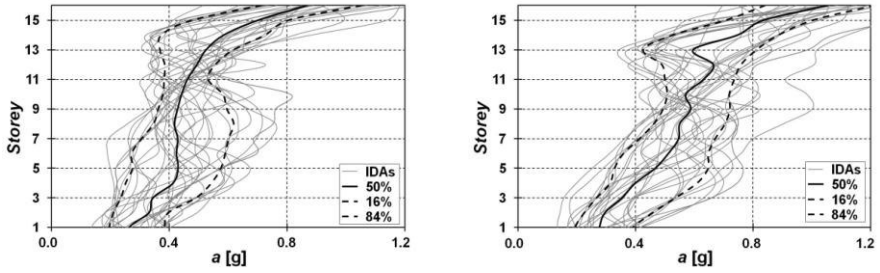

16-storeys

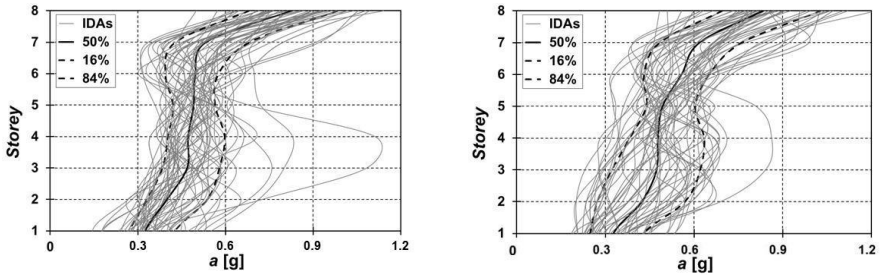

8-storeys

Fig. 4.22. Peak storey accelerations - NC

REFERENCES

- EN 1998-1-1. Eurocode 8. 2004. Design of structures for earthquake resistance – Part 1: General rules, seismic actions and rules for buildings. CEN.
- EN 1998-1-3. Eurocode 8. 2004. Design of structures for earthquake resistance – Part 1: General rules, seismic actions and rules for buildings. CEN.
- Grecea D, Dinu F, Dubina D. 2004. Performance criteria for MR steel frames in seismic zones. J Construct Steel Res; 60:739-749.
- EN 1993-1, Eurocode 3. 2005. Design of steel structures – Part 1-1: General rules and rules for buildings. CEN.
- EN 1994-1, Eurocode 4. 2004. Design of composite steel and concrete structures – Part 1-1: General rules and rules for buildings. CEN.
- SeismoStruct, Version 5.0.5. Seismosoft – Earthquake Engineering Software Solution.
- Spacone E., Ciampi V., Filippou FC. 1996. Mixed formulation of nonlinear beam finite element. ComputStruct; 58(I):71-83.
- Calabrese A, Almeida JP, Pinho R. 2010. Numerical issues in distributed inelasticity modelling of RC frame elements for seismic analysis. J. Earthq. Eng; 14(1):38-68.
- Martinez-Rueda JE, Elnashai AS. 1997. Confined concrete model under cyclic load. MaterStruct;30: 139-147.
- Mander JB, Priestley MJN, Park R. 1988. Theorical stress-strain model for confined concrete. JStruct Eng;8(114):1804-1826.
- Susantha KAS, Ge H, Usami T. 2001. Unixial stress-strain relationship of concrete confined by various shaped steel tubes. Eng Struct; 23(10): 1331-1347.
- Menegotto M, Pinto PE. 1973. Method of analysis for cyclically loaded R.C. plane frames including changes in geometry and non-elastic behaviour of elements under combined normal force and bending. In: Symposium on the Resistance and Ultimate Deformability of Structures Acted on by Well Defined Repeated Loads.

- EN 1992-1-1, Eurocode 2. 2004 Design of concrete structures - Part 1-1: General rules and rules for buildings. CEN.
- RFSR-CT-2007-00039. 2013. Optimizing the seismic performance of steel and steel-concrete structures by standardizing material quality control (OPUS). ISBN: 978-92-79-29037-4, DOI: 10.2777/79330
- Abramowitz M, Stegun IA. 1964. Handbook of Mathematical Functions, National Bureau of Standards, Applied Math. Series.
- D'Aniello M, Landolfo R, Piluso V, Rizzano G. 2012. Ultimate Behaviour of Steel Beams under Non-Uniform Bending. J Construct Steel Res; 78:144–158.
- D'Aniello M, La Manna Ambrosino G, Portioli F, Landolfo R. 2013. Modelling aspects of the seismic response of steel concentric braced frames. Steel and Composite Structures;15(5): 539-566.
- Elghazoulli AY. 2005. Assessment of capacity design approaches for steel-framed structures. JSteel Struct; 5: 465-475.
- Fulop L. 210. Selection of earthquake records for the parametric analysis.Research report VTT-R-03238-10, VTT, Espoo.

5 DUAL ECCENTRICALLY BRACED FRAME WITH REMOVABLE LINKS

5.1 INTRODUCTION

Different solutions and strategies have been developed in the last decades with the aim to minimize the damage of structures under moderate to strong earthquakes. Some solutions are based either on isolation or on active and semi-active structural control. Other strategies are based on supplemental damping, i.e. viscous, friction, or yielding dampers. All these solutions require a specialized knowledge at design stage.

The most convenient approach could be to carry on a conventional design but with the dissipative members realised to be removable, allowing replacement of the dissipative elements damaged. To follow this way the structure have to be repairable, in addition to constraining inelastic deformations to removable dissipative members, the permanent drifts should be eliminated.

Application of the concept of removable dissipative members to eccentrically braced frames (EBFs), where links act as dissipative zones, are presented in Stratan and Dubina (2004) and Dubina et al. (2008). The connection of the link to the beam is realized by a flush end-plate and high-strength friction grip bolts. According to this approach it is possible design the removable links using simple methods available to structural engineers.

The re-centring effect is obtained combining eccentrically braced frames (EBFs) with moment-resisting frames (MRFs). The elastic response of the MRF provides the restoring forces after the link removal. To pursue this goal the MRFs should remain in the elastic range; and the use of high-strength steel could simplified this objective. When the deformations are too large, it is possible to slowly release the residual stresses and deformations in the link by removing part of the link through flame cutting prior to removing the bolts, reducing the residual stresses in the link.

An important aspect to analyse is the interaction between the removable link and the concrete slab. On one hand, the concrete slab can modify the link shear capacity but on the other hand, large link deformations can damage the concrete slab. One possible solution is to disconnect the removable link from the reinforced concrete slab, with an additional secondary beam placed in parallel with the beam containing the link. In the case in which there is a connection between the reinforced concrete slab and the removable link, a concrete damage it's possibile. In this case, it would be necessary to repair locally the slab after a damaging earthquake, in addition to replacing the removable link.

5.2 STRUCTURE DESIGN

A medium rise prototype structure was considered, see fig. 5.1. The building has 3 spans of 6 meters and 5 bays of 6 meters. The building has 3 storeys of 3.5 meters each.

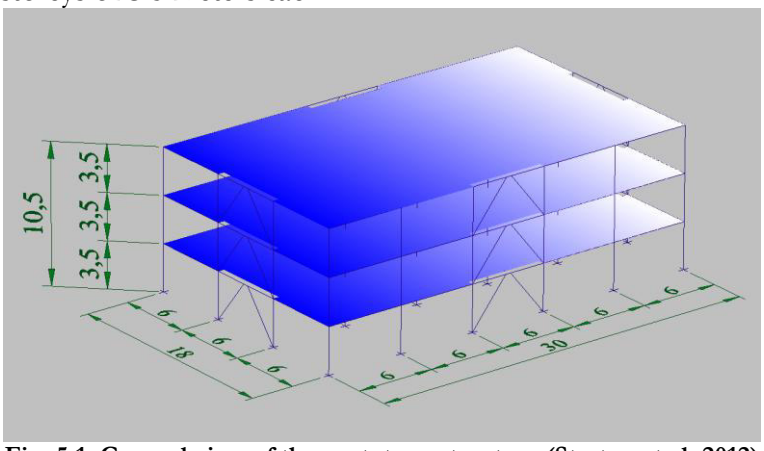

Fig. 5.1 General view of the prototype structure (Stratan et al. 2012)

The main lateral load resisting system is composed of eccentrically braced frames, located on the perimeter. Then, there are 4 moment resisting frames on transversal directions and 10 moment resisting frames on longitudinal direction, to assure the restoring forces after an earthquake. All other beams have pinned ends and are composite steel-concrete beams. The columns are fixed at the base. Columns are made of HEA240 profiles. Beams in the moment resisting frames are made of IPE240. Braces are made of HEB200 profiles and the beams in the braced frames of HEA240, while links are made of welded H sections

230x170x12x7 mm (for the first two lower levels, where the dimensions represent: h x b x t_f x t_w) and 230x120x12x4 mm (for the last upper level), see Figure 5.2 b.

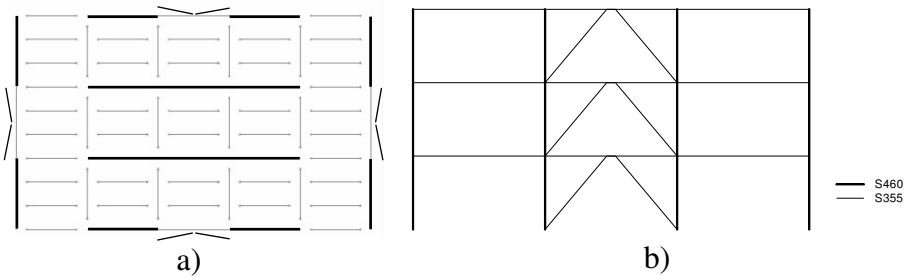

Fig. 5.2 Structural configuration: plan view (a); transversal end frame (b)

Considering that in the transversal direction the lateral force resisting system is located on the perimeter frames only, and in order to reduce the cost of the experimental specimen, the latter is to be composed of the two end frames only (see Figure 5.3)

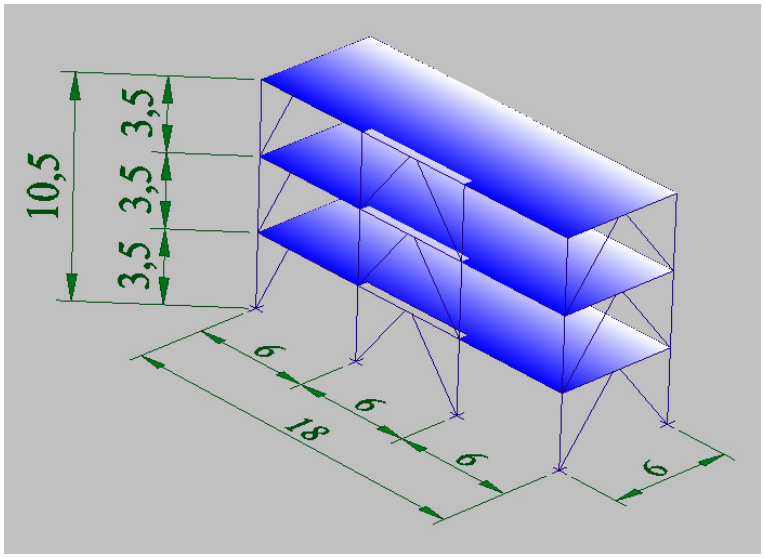

Fig. 5.3 General view of the test structure (Stratan et al. 2012)

5.3 DESIGN BRIEF

The design was carried out according to EN1990, EN1991, EN1992, EN1993, EN1994 and EN1998. A 4.9 kN/m^2 dead load and 3.0 kN/m^2

live load were considered. The building is analysed for stiff soil conditions, characterised by 0.19g peak ground acceleration and T_C=0.6s. A behaviour factor q=4 (ductility class M) and inter-storey drift limitation of 0.0075 of the storey height are used. The columns are fabricated of high strength steel S460, while all the other elements are fabricated of mild carbon steel S355, except links that are of S235 steel (with a $f_{y,max}$=298 N/mm2). For what concern the loads evaluation a permanent G_k=4.90 kN/m^2 (according to EN1991) and live load Q_k=3.0 kN/m^2 (according to EN 1991, office areas) is assumed. According to the Romanian Code NP-082-04 the design wind pressure is:

0.655 kN/m^2 on the windward wall

0.261 kN/m^2 on the leeward wall

For what concern the seismic combinations it's assumed

Ultimate Limit State Combinations:

1. F-ULS: 1.35 G_k + 1.5 Q_k
2. F-ULS-W: 1.35 G_k + 1.5 W_k + 1.05 Q_k
3. F-ULS-Q: 1.35 G_k + 1.5 Q_k + 1.05W_k

Serviceability Limit State Combinations:

1. F-SLS: 1.00 G_k + 1.00 Q_k
2. F-SLS-W: 1.00 G_k + 1.00 W_k + 0.7 Q_k
3. F-SLS-Q: 1.00 G_k + 1.00 Q_k + 0.7 W_k

Seismic design situation

Combination used to design the dissipative members:

DISIP: 1.00 G_k + 0.30 Q_k + A_{ek}

Combination used to design the non - dissipative members:

NEDISIP: 1.00 G_k + 0.30 Q_k + $\Omega^{tot} * A_{ek}$

$\Omega^{tot} = 1.1 * \gamma_{ov} * \Omega^{M}$

Serviceability Limit State Combination:

S-SLS: 1.00 G_k + 0.30 Q_k + $\nu * q * A_{ek}$

q = 4 and ν = 0.5 (importance class II of the building)

in which:

G_k = permanent load

Q_k = live load

W_k = transversal wind

A_{ek} = earthquake

5.4 MODEL FOR SHEAR DETACHABLE LINK

On the basis of tests carried out by Stratan and Dubina (see fig. 5.4), the total link deformation is given by the shear distortion of the link panel, the rotation in the two connections and by the slip in the connections.

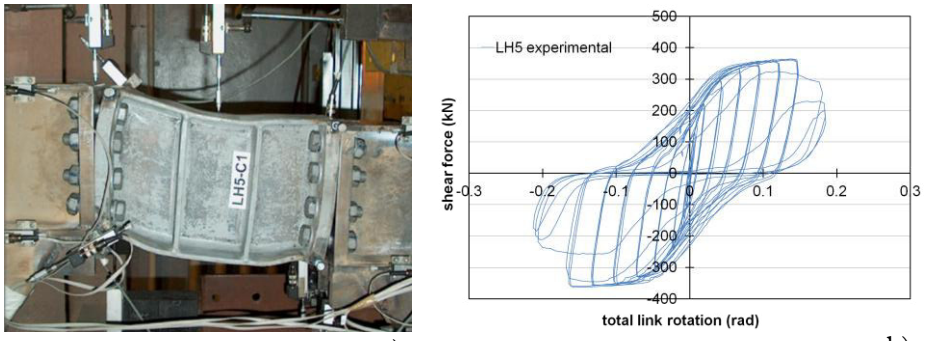

a) b)

Fig. 5.4 General view of the test structure (Stratan and Dubina 2004)

Introducing the notation $\theta_M=(\theta_S+\theta_J)/2$, which represents the average connection rotation, link rotation may be determined as (see. fig. 5.5):

$$\gamma_L = \gamma + \theta_M$$

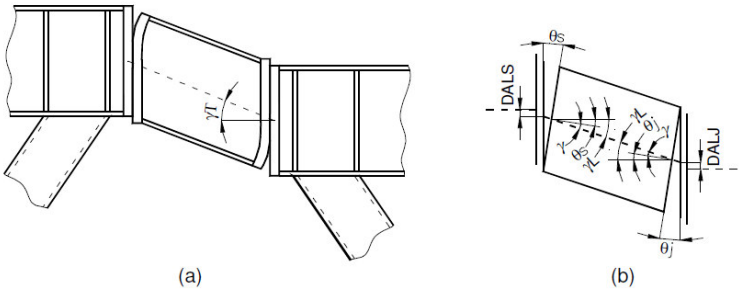

Fig. 5.5 Deformation of a bolted link (Stratan and Dubina 2004)

As observed by these tests and also recently confirmed by Mazzolani et al 2009, but also by more recent tests by Mansur et al 2008, the connection design is critical for replaceable links. Mazzolani tested deatachable links with rigid end connections + axial restraints. Very large shear overstrength was observed.

Mansur et al (2008) tested detachable links using 2 types of joints:

- end plate connections,
- back-to-back channels with eccentrically loaded web connections.

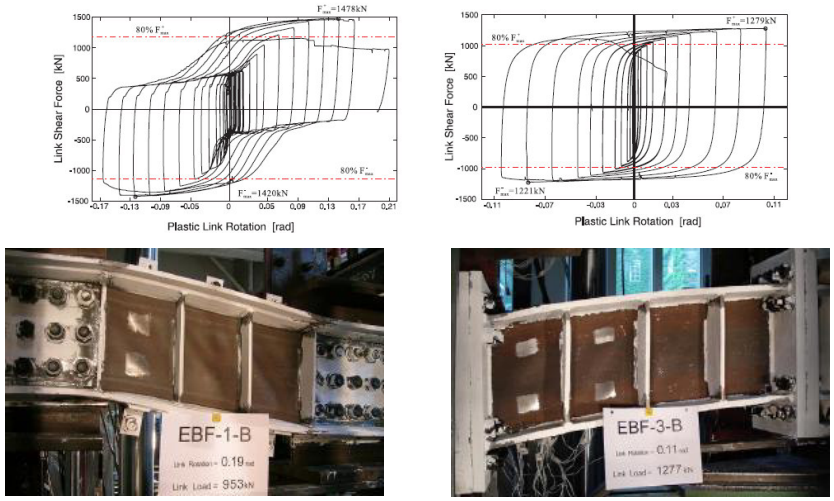

Fig 5.6 Experimental tests from Mansur et al. (2008)

For both structural systems, the end plate links exhibited higher energy dissipation capacity than the double channel links. Because of their

connection flexibility, on the other hand, the double channel links enjoyed significantly higher rotational capacity.
In conclusion, the link model should account for shear distortion of the link panel, rotation in the two connections and slip in the connections. Particularly, shear distortion of the link panel may be accounted for using Bilinear Kinematic or Ramberg-Osgood model; the slip in the connections may be accounted for as an equivalent stiffness reduction, introducing also pinching in the cyclic response and finally the flexural deformability of link end connection should be introduced considering both elastic and post-elastic behaviour.
The slip in the connections may be accounted for as an equivalent stiffness reduction, introducing also pinching in the cyclic response (fig. 5.7)

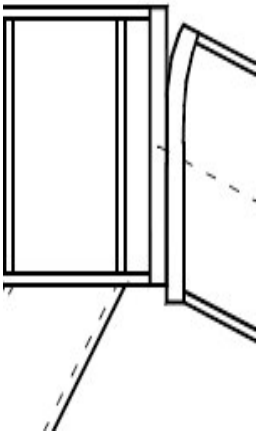

Fig 5.7 Slip connection (Stratan and Dubina 2004)

The shear spring must be modified to accounted for the slip. To match the experimental stiffness it is necessary to reduce the initial rigidity. Calibrated stiffness is about 1/4 times the theoretical for perfect restraints.

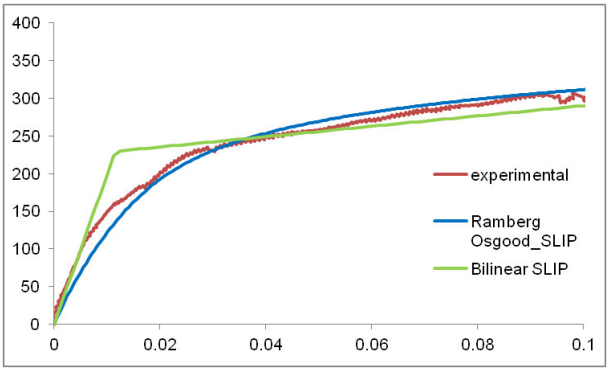

Fig 5.8 link numerical curve

The link end connections are flush-end joints subjected to large flexural+shear interaction. If the parts connected to the links are very stiff (as a RC slab) the end connections are subjected to axial forces too.
The flexural stiffness of the joint may be calculated using EN1993:1-8. It is necessary to account for pinching and strength/stiffness degradation phenomena. The flexural deformability of link end connection + pinching has been accounted for using the mathematical model by M.V. Sivaselvan, A. M. Reinhorn (2000). The parameters have been calibrated using a trial and error procedure such as in fig. 5.9.

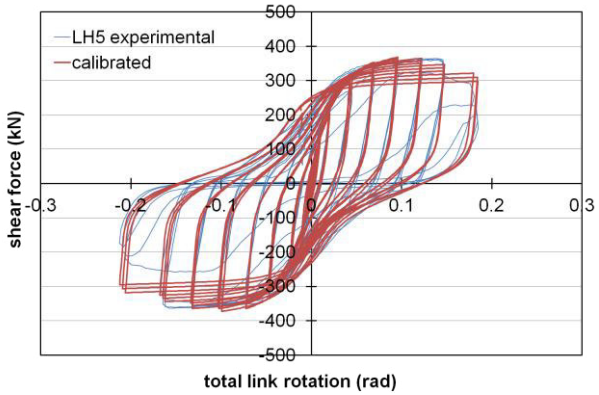

Fig 5.9 Hysteretic link curve

5.5 PRELIMINARY RESULT

Seven natural accelerograms scaled according to EN 1998-1:2004 have been used to perform nonlinear dynamic analyses (see. Tab. 5.1 and fig. 5.10)

Record code	Earthquake Name	Date	Station Name	Station Country
000333XA	Alkion	24.02.1981	Korinthos-OTE Building	Greece
000600XA	Umbria Marche	26.09.1997	Castelnuovo-Assisi	Italy
001255XA	Izmit	17.08.1999	Heybeliada-Senatoryum	Turkey
004343YA	Izmit	17.08.1999	Istanbul-Zeytinburnu	Turkey
007097YA	Ishakli	03.02.2002	Afyon-Bayindirlik ve Iskan Mudurlugu	Turkey
013009XA	Olfus	29.05.2008	Ljosafoss-Hydroelectric Power Station	Iceland
013010XA	Olfus	29.05.2008	Selfoss-City Hall	Iceland

Tab. 5.1 the selected accelerograms.

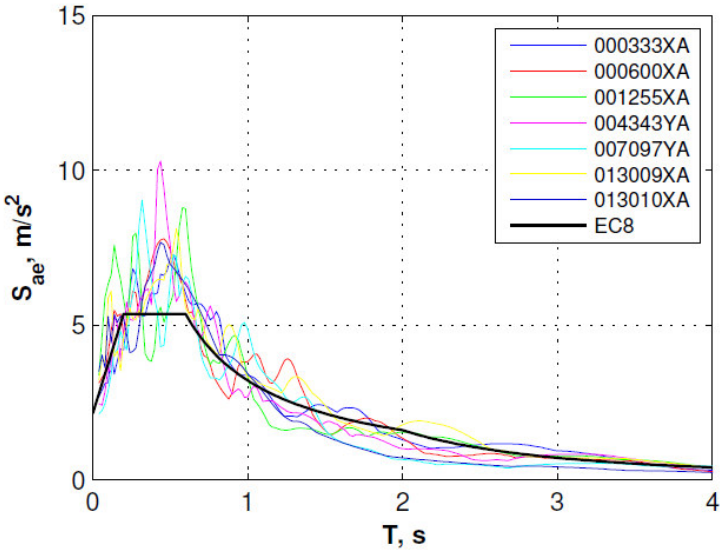

Fig 5.10 Response spectra of the selected records

IDAs have been carried out assuming a tangential stiffness Rayleigh damping (2% for 1st and 2nd mode). According to EN 1998-1:2004, limit states to be considered are those indicated in tab. 5.2.

In fig. 5.11 is reported the finite element model.

Tab. 5.2 link numerical curve

Limit state	Return period, years	Probability of exceedance	a_g/a_{gr}
Full operation (FO)	7	75% / 10 years	0.25
Damage Limitation (DL / SLS)	95	10% / 10 years	0.59
Significant Damage (SD / ULS)	475	10% / 50 years	1.00
Near Collapse (NC)	2475	2% / 50 years	1.72

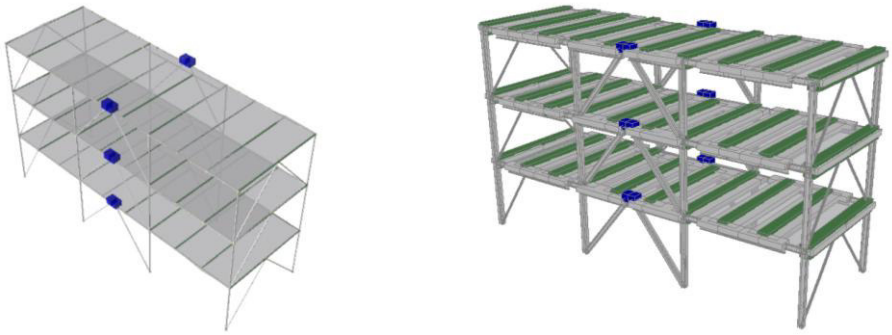

Fig 5.11 Finite element model

Preliminary objectives are related to the check overall performance of the structure, to evaluate permanent interstorey drifts, to evaluate the accelerogram leading to the largest permanent displacements is to be selected for PSD test and to check deformation demands in links. For what concern FO and DL limit states it's noted that drift demand and storey acceleration are very small. The mockup is basically elastic. Some yielding in links belonging to 1st storey are observed, but no damage can be actually recognized. The Severe Damage and Near Collapse limit states are the most interesting. In fact, in SD all links at 1st and 2nd storey plastify, but small residual drift ratios can be recognized while in NC limit state all links plastify and larger residual drift ratios are recognizable. In fig. 5.12 and 5.13 are depicted the maximum base shear and the maximum acceleration for each record, respectively.

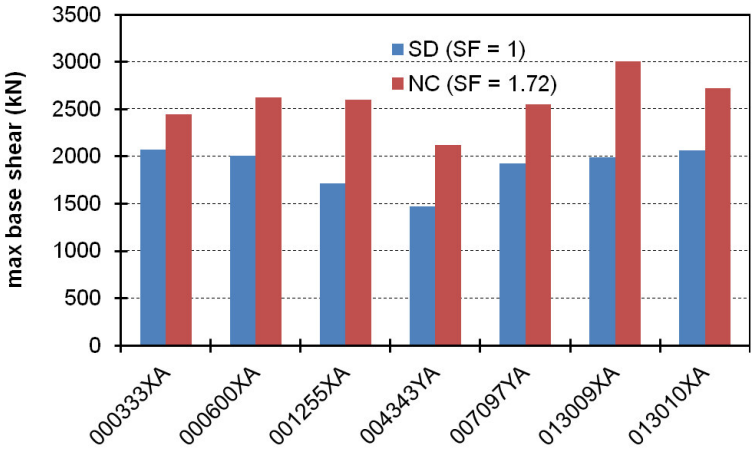

Fig 5.12 Maximum base shear for each record

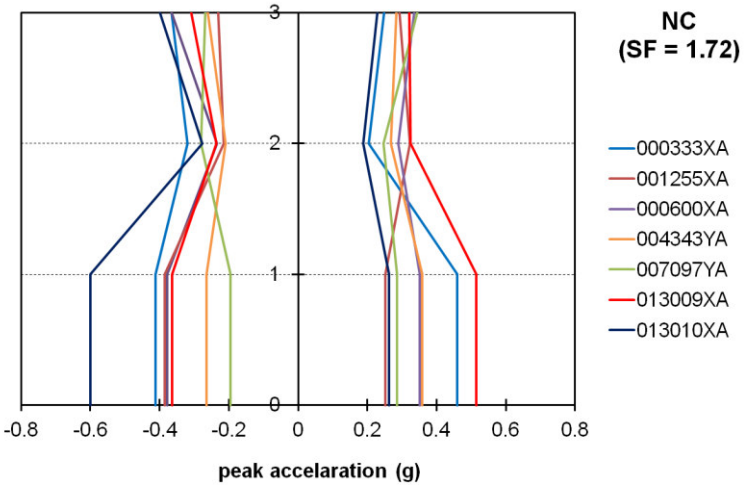

Fig 5.13 Maximum acceleration each record

In fig. 5.14 are depicted the peak interstorey drift ration for each record for SD and NC limit state

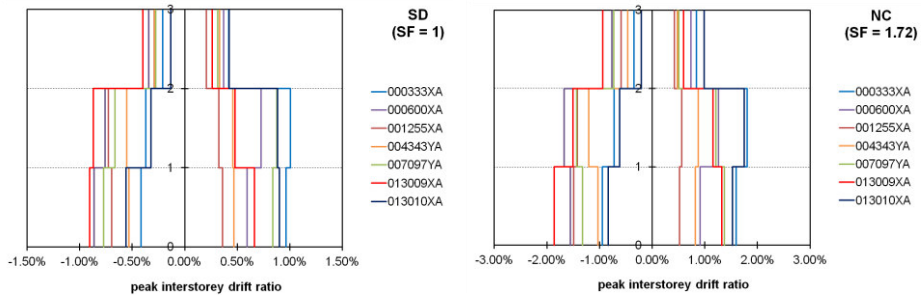

Fig 5.14 Peak interstorey drift ratio

For what concern the residual iterstorey drift ratio (fig. 5.15) the records inducing the largest residual interstorey drift ratios (about 0.15%) are the following:

000333XA - 013009XA - 013010XA

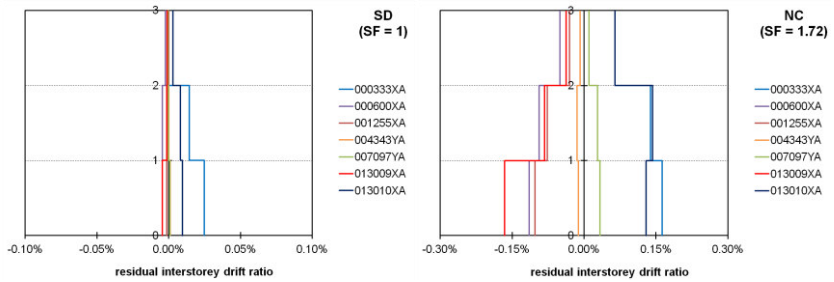

Fig 5.15 Residual interstorey drift ratio

Finally, referring to the total link rotation (shear link + connections) it's noted that it is always smaller than 0.10 << 0.14 rad, according to tests by Stratan & Dubina (2004), such as in fig. 5.16.

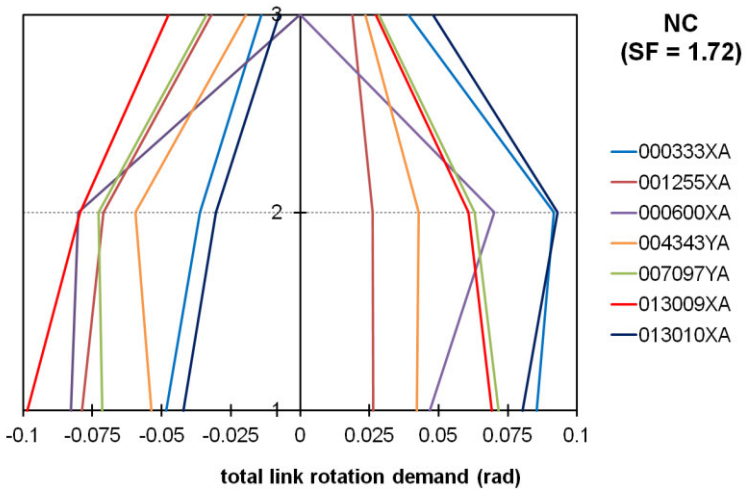

Fig 5.16 Residual interstorey drift ratio

REFERENCES

- EN 1998-1-1. Eurocode 8. 2004. Design of structures for earthquake resistance – Part 1: General rules, seismic actions and rules for buildings. CEN.
- Dubina, D., Stratan, A., Dinu, F. (2008). "Dual high-strength steel eccentrically braced frames with removable links". Earthquake Engineering & Structural Dynamics, Vol. 37, No. 15, p. 1703-1720.
- Stratan, A. and Dubina, D. (2004). "Bolted links for eccentrically braced steel frames". Proc. of the Fifth AISC / ECCS International Workshop "Connections in Steel Structures V. Behaviour, Strength & Design", June 3-5, 2004. Ed. F.S.K. Bijlaard, A.M. Gresnigt, G.J. van der Vegte. Delft University of Technology, The Netherlands, pp. 223-232
- EN 1990-1-1. Eurocode 0. 2006. Basis of structural design. CEN.
- F. M. Mazzolania, G. Della Corteb & M. D'Aniello. 2009. Experimental analysis of steel dissipative bracing systems for seismic upgrading. Journal of Civil Engineering and Management. Vol. 15, Issue 1, 7-19
- Mansour, N., Christopoulos, C, and Tremblay, R. (2011). Experimental Validation of Replaceable Shear Links for Eccentrically Braced Steel Frames. J. Struct. Eng. 137, 1141.
- Sivaselvan, M.V. and Reinhorn, A.M. (2000). "Hysteretic models for deteriorating inelastic structures", Journal of Engineering Mechanics-ASCE, 126(6), 633-640 127(11) 1201-1202

6 CONCLUSION

6.1 CONCLUSION

A parametric study based on nonlinear static and dynamic analyses has been presented in order to evaluate the seismic performance of dual-steel eccentric braced frames in simple and dual configuration designed according to EN1998-1. High strength steel grade S460 and S690 have been used for columns and mild carbon steel S355 for beams.
The seismic performance-based evaluation has been carried out considering three limit states according to EN1998-3, namely damage limitation (DL), significant damage (SD) and near collapse (NC).
The use of HSS showed to be efficient to guarantee the weak-beam/strong-column behaviour.
Nonlinear dynamic analyses showed that the frames have a seismic demand fairly below the proposed limit for DL, SD and NC states. In particular, at DL limit state the most of frames behave in elastic field. This result is mainly due to the design oversizing, that is a direct consequence of the design procedure implemented in EN1998-1.
The median peak storey accelerations range between 2 to 3 times the design PGA. Therefore, significant amplification effects can occur and should be accounted for preserve the integrity of facilities and non-structural elements.
The Dual EBFs showed smaller peak and residual interstorey drift ratios than simple EBFs, and the dual steel-dual frame concept is the most favourable combination of design strategy.
The behaviour factors obtained from incremental dynamic analyses (IDAs) for SD limit state are smaller than the code value, because of the premature brace buckling. This result highlight that the current codified requirements do not guarantee a ductile seismic performance.
Analogous results have been obtained at NC limit states, where the buckling of braces is the crucial aspect imparing the overall performance.
An alternative design criteria has been presented to avoid the brace buckling. The analyses showed that the frames designed on the basis of

the updated criteria may experience behaviour factor larger than those suggested by the code.
The numerical preparatory study addressed to design the experimental setup for a real scale steel building made of dual Eccentric braced frame having removable links showed that dual systems may effectively provide adequate recenter capacity even in case of significant damage by simply removing the shear links. In addition, the removal of damaged links is feasible producing small accelerations and small couterstroke.

ANNEX 1

The cross sections of the members obtained from the design of the frames performed by GIPAC, UNINA and VTT are reported

EBF 1.1.1.1.1								
Storey	**Columns**		**Outer Beam**		**Inner Beam/Link**		**Brace**	
[-]	**Material**	**Profile**	**Material**	**Profile**	**Material**	**Profile**	**Material**	**CHS**
1	S460	HEB 240	S355	IPE 270	S355	HEB 240	S355	168.3x10
2		HEB 240		IPE 270		HEB 220		168.3x8
3		HEB 240		IPE 270		HEB 220		168.3x6.3
4		HEB 240		IPE 270		HEB 200		168.3x6.3
5	S355	HEB 180		IPE 270		HEB 180		168.3x5
6		HEB 180		IPE 270		HEB 180		139.7x8
7		HEB 180		IPE 270		HEB 160		139.7x6
8		HEB 180		IPE 270		HEA 160		139.7x3.6

EBF 1.1.1.1.2								
Storey	**Columns**		**Outer Beam**		**Inner Beam/Link**		**Brace**	
[-]	**Material**	**Profile**	**Material**	**Profile**	**Material**	**Profile**	**Material**	**CHS**
1	S460	HEB 280	S355	IPE 270	S355	HEB 240	S355	168.3x8
2		HEB 280		IPE 270		HEB 220		168.3x8
3		HEB 280		IPE 270		HEB 200		168.3x6.3
4		HEB 280		IPE 270		HEB 180		168.3x5
5	S355	HEB 180		IPE 270		HEB 180		168.3x5
6		HEB 180		IPE 270		HEB 180		139.7x8
7		HEB 180		IPE 270		HEB 160		139.7x6
8		HEB 180		IPE 270		HEA 160		139.7x3.6

EBF 1.1.1.2.1								
Storey	**Columns**		**Outer Beam**		**Inner Beam/Link**		**Brace**	
[-]	**Material**	**Profile**	**Material**	**Profile**	**Material**	**Profile**	**Material**	**CHS**
1	S460	HEB 320	S355	IPE 270	S355	HEB 360	S355	219.1x10
2		HEB 320		IPE 270		HEB 360		219.1x10
3		HEB 320		IPE 270		HEB 340		219.1x10
4		HEB 320		IPE 270		HEB 320		193.7x10
5	S355	HEB 300		IPE 270		HEB 300		193.7x10
6		HEB 300		IPE 270		HEB 280		168.3x10
7		HEB 300		IPE 270		HEB 220		168.3x8
8		HEB 300		IPE 270		HEB 160		139.7x6.3

EBF 1.1.1.2.2								
Storey	**Columns**		**Outer Beam**		**Inner Beam/Link**		**Brace**	
[-]	**Material**	**Profile**	**Material**	**Profile**	**Material**	**Profile**	**Material**	**CHS**
1	S460	HEM 300	S355	IPE 270	S355	HEB 340	S355	193.7x12
2		HEM 300		IPE 270		HEB 340		193.7x12
3		HEM 300		IPE 270		HEB 320		193.7x12
4		HEM 300		IPE 270		HEB 300		193.7x10
5	S355	HEB 300		IPE 270		HEB 300		193.7x8
6		HEB 300		IPE 270		HEB 260		193.7x6.3
7		HEB 300		IPE 270		HEB 220		168.3x6.3
8		HEB 300		IPE 270		HEB 160		139.7x6

EBF 1.1.2.1.1								
Storey	**Columns**		**Outer Beam**		**Inner Beam/Link**		**Brace**	
[-]	**Material**	**Profile**	**Material**	**Profile**	**Material**	**Profile**	**Material**	**CHS**
1	S460	HEB 460	S355	IPE 360	S355	HEB 360	S355	244.5x10
2		HEB 460		IPE 360		HEB 360		244.5x10
3		HEB 460		IPE 360		HEB 340		244.5x10
4		HEB 460		IPE 360		HEB 320		219.1x10
5	S355	HEB 280		IPE 360		HEB 280		219.1x10
6		HEB 280		IPE 360		HEB 280		197.3x10
7		HEB 280		IPE 360		HEB 220		197.3x8
8		HEB 280		IPE 360		HEB 180		168.3x8

EBF 1.1.2.1.2								
Storey	**Columns**		**Outer Beam**		**Inner Beam/Link**		**Brace**	
[-]	**Material**	**Profile**	**Material**	**Profile**	**Material**	**Profile**	**Material**	**CHS**
1	S460	HEM 300	S355	IPE 360	S355	HEB 360	S355	244.5x10
2		HEM 300		IPE 360		HEB 360		244.5x10
3		HEM 300		IPE 360		HEB 360		244.5x10
4		HEM 300		IPE 360		HEB 340		219.1x10
5	S355	HEB 280		IPE 360		HEB 280		219.1x10
6		HEB 280		IPE 360		HEB 280		197.3x10
7		HEB 280		IPE 360		HEB 240		197.3x10
8		HEB 280		IPE 360		HEB 180		197.3x5

EBF 1.1.2.2.1								
Storey	**Columns**		**Outer Beam**		**Inner Beam/Link**		**Brace**	
[-]	**Material**	**Profile**	**Material**	**Profile**	**Material**	**Profile**	**Material**	**CHS**
1	S460	HEM 300	S355	IPE 360	S355	HEB 400	S355	273x10
2		HEM 300		IPE 360		HEB 400		273x10
3		HEM 300		IPE 360		HEB 360		273x10
4		HEM 300		IPE 360		HEB 340		244.5x10
5	S355	HEB 300		IPE 360		HEB 320		219.1x12
6		HEB 300		IPE 360		HEB 280		219.1x10
7		HEB 300		IPE 360		HEB 240		193.7x10
8		HEB 300		IPE 360		HEB 180		168.3x8

EBF 1.1.2.2.2								
Storey	**Columns**		**Outer Beam**		**Inner Beam/Link**		**Brace**	
[-]	**Material**	**Profile**	**Material**	**Profile**	**Material**	**Profile**	**Material**	**CHS**
1	S460	HEM 340	S355	IPE 360	S355	HEB 400	S355	273x10
2		HEM 340		IPE 360		HEB 400		273x10
3		HEM 340		IPE 360		HEB 360		244.5x12
4		HEM 340		IPE 360		HEB 340		244.5x10
5	S355	HEB 300		IPE 360		HEB 320		244.5x10
6		HEB 300		IPE 360		HEB 280		219.1x10
7		HEB 300		IPE 360		HEB 240		193.7x10
8		HEB 300		IPE 360		HEB 180		168.3x8

EBF 1.2.2.1.2								
Storey	**Columns**		**Outer Beam**		**Inner Beam/Link**		**Brace**	
[-]	**Material**	**Profile**	**Material**	**Profile**	**Material**	**Profile**	**Material**	**CHS**
1	S690	HEM 280	S355	IPE 360	S355	HEB 360	S355	244.5x12
2		HEM 280		IPE 360		HEB 340		244.5x10
3		HEM 280		IPE 360		HEB 320		219.1x12
4		HEM 280		IPE 360		HEB 300		219.1x10
5	S355	HEB 280		IPE 360		HEB 280		219.1x10
6		HEB 280		IPE 360		HEB 280		197.3x10
7		HEB 280		IPE 360		HEB 220		197.3x8
8		HEB 280		IPE 360		HEB 180		168.3x8

EBF 1.2.2.2.2								
Storey	**Columns**		**Outer Beam**		**Inner Beam/Link**		**Brace**	
[-]	**Material**	**Profile**	**Material**	**Profile**	**Material**	**Profile**	**Material**	**CHS**
1	S690	HEM 300	S355	IPE 360	S355	HEB 400	S355	273x10
2		HEM 300		IPE 360		HEB 400		273x10
3		HEM 300		IPE 360		HEB 360		273x10
4		HEM 300		IPE 360		HEB 340		244.5x10
5	S355	HEB 300		IPE 360		HEB 320		244.5x10
6		HEB 300		IPE 360		HEB 280		193.7x12
7		HEB 300		IPE 360		HEB 240		193.7x10
8		HEB 300		IPE 360		HEB 180		168.3x8

EBF 2.1.2.1.1								
Storey	**Columns**		**Outer Beam**		**Inner Beam/Link**		**Brace**	
[-]	**Material**	**Profile**	**Material**	**Profile**	**Material**	**Profile**	**Material**	**CHS**
1	S460	PRS 700x400x20x50	S355	IPE 360	S355	HEB 360	S355	355.6x8
2		PRS 700x400x20x50		IPE 360		HEM 360		457x10
3		PRS 700x400x20x50		IPE 360		HEM 340		406.4x10
4		PRS 700x400x20x50		IPE 360		HEM 320		406.4x10
5		HEM 650		IPE 360		HEM 300		355.6x10
6		HEM 650		IPE 360		HEM 300		355.6x10
7		HEM 650		IPE 360		HEB 450		323.9x10
8		HEM 650		IPE 360		HEB 400		323.9x10
9		HEB 450		IPE 360		HEB 400		273x12
10		HEB 450		IPE 360		HEB 400		273x10
11		HEB 450		IPE 360		HEB 360		244.5x10
12		HEB 450		IPE 360		HEB 340		244.5x10
13	S355	HEB 300		IPE 360		HEB 340		219.1x12
14		HEB 300		IPE 360		HEB 300		219.1x10
15		HEB 300		IPE 360		HEB 240		193.7x10
16		HEB 300		IPE 360		HEB 200		193.7x6

EBF 2.1.2.1.2								
Storey	**Columns**		**Outer Beam**		**Inner Beam/Link**		**Brace**	
[-]	**Material**	**Profile**	**Material**	**Profile**	**Material**	**Profile**	**Material**	**CHS**
1	S460	PRS 700x450x30x55	S355	IPE 360	S355	HEB 360	S355	355.6x8
2		PRS 700x450x30x55		IPE 360		HEM 360		457x10
3		PRS 700x450x30x55		IPE 360		HEM 320		406.4x10
4		PRS 700x450x30x55		IPE 360		HEM 320		406.4x10
5		PRS 600x400x20x40		IPE 360		HEM 300		355.6x10
6		PRS 600x400x20x40		IPE 360		HEB 450		355.6x10
7		PRS 600x400x20x40		IPE 360		HEB 450		323.9x10
8		PRS 600x400x20x40		IPE 360		HEB 400		273x12
9		HEM 300		IPE 360		HEB 400		273x12
10		HEM 300		IPE 360		HEB 400		273x10
11		HEM 300		IPE 360		HEB 360		273x10
12		HEM 300		IPE 360		HEB 340		244.5x10
13	S355	HEB 300		IPE 360		HEB 320		244.5x10
14		HEB 300		IPE 360		HEB 300		219.1x10
15		HEB 300		IPE 360		HEB 240		219.1x8
16		HEB 300		IPE 360		HEB 200		193.7x6

EBF 2.1.2.2.1								
Storey	**Columns**		**Outer Beam**		**Inner Beam/Link**		**Brace**	
[-]	**Material**	**Profile**	**Material**	**Profile**	**Material**	**Profile**	**Material**	**CHS**
1	S460	PRS 750x470x35x75	S355	IPE 360	S355	HEB 500	S355	406.4x10
2		PRS 750x470x35x75		IPE 360		HEM 550		457x12
3		PRS 750x470x35x75		IPE 360		HEM 550		457x16
4		PRS 750x470x35x75		IPE 360		HEM 550		457x12.5
5		PRS 650x420x20x50		IPE 360		HEM 550		457x12.5
6		PRS 650x420x20x50		IPE 360		HEM 500		406.4x16
7		PRS 650x420x20x50		IPE 360		HEM 450		406.4x12.5
8		PRS 650x420x20x50		IPE 360		HEM 400		406.4x12
9		HEB 650		IPE 360		HEM 400		406.4x12
10		HEB 650		IPE 360		HEM 340		355.6x12.5
11		HEB 650		IPE 360		HEM 320		323.9x12.5
12		HEB 650		IPE 360		HEB 450		323.9x12
13	S355	HEB 300		IPE 360		HEB 400		273x12
14		HEB 300		IPE 360		HEB 360		273x10
15		HEB 300		IPE 360		HEB 320		219.1x10
16		HEB 300		IPE 360		HEB 220		193.7x6.3

EBF 2.1.2.2.2								
Storey	**Columns**		**Outer Beam**		**Inner Beam/Link**		**Brace**	
[-]	**Material**	**Profile**	**Material**	**Profile**	**Material**	**Profile**	**Material**	**CHS**
1	S460	PRS 800x500x34x75	S355	IPE 360	S355	HEM 400	S355	406.4x16
2		PRS 800x500x34x75		IPE 360		HEM 500		457x12
3		PRS 800x500x34x75		IPE 360		HEM 500		457x12
4		PRS 800x500x34x75		IPE 360		HEM 500		457x12
5		PRS 700x450x22x50		IPE 360		HEM 450		457x12
6		PRS 700x450x22x50		IPE 360		HEM 450		457x12
7		PRS 700x450x22x50		IPE 360		HEM 450		406.4x12.5
8		PRS 700x450x22x50		IPE 360		HEM 400		355.6x12.5
9		HEM 600		IPE 360		HEM 400		355.6x12.5
10		HEM 600		IPE 360		HEM 360		323.9x12.5
11		HEM 600		IPE 360		HEM 360		323.9x12.5
12		HEM 600		IPE 360		HEB 450		323.9x10
13	S355	HEB 300		IPE 360		HEB 400		323.9x10
14		HEB 300		IPE 360		HEB 360		244.5x10
15		HEB 300		IPE 360		HEB 300		219.1x10
16		HEB 300		IPE 360		HEB 220		168.3x10

EBF 2.2.2.1.2								
Storey	**Columns**		**Outer Beam**		**Inner Beam/Link**		**Brace**	
[-]	**Material**	**Profile**	**Material**	**Profile**	**Material**	**Profile**	**Material**	**CHS**
1	S690	PRS 680x425x20x45	S355	IPE 360	S355	HEB 360	S355	355.6x10
2		PRS 680x425x20x45		IPE 360		HEM 360		457x10
3		PRS 680x425x20x45		IPE 360		HEM 340		406.4x10
4		PRS 680x425x20x45		IPE 360		HEM 320		406.4x10
5		PRS 550x350x15x35		IPE 360		HEM 300		355.6x10
6		PRS 550x350x15x35		IPE 360		HEM 300		355.6x10
7		PRS 550x350x15x35		IPE 360		HEB 450		323.9x10
8		PRS 550x350x15x35		IPE 360		HEB 400		273x12
9		HEM 300		IPE 360		HEB 400		273x12
10	S460	HEM 300		IPE 360		HEB 400		273x10
11		HEM 300		IPE 360		HEB 360		273x10
12		HEM 300		IPE 360		HEB 340		244.5x10
13	S355	HEB 300		IPE 360		HEB 340		244.5x10
14		HEB 300		IPE 360		HEB 300		219.1x10
15		HEB 300		IPE 360		HEB 240		193.7x10
16		HEB 300		IPE 360		HEB 200		193.7x6

EBF 2.2.2.2.2								
Storey	**Columns**		**Outer Beam**		**Inner Beam/Link**		**Brace**	
[-]	**Material**	**Profile**	**Material**	**Profile**	**Material**	**Profile**	**Material**	**CHS**
1	S690	PRS 650x450x32x60	S355	IPE 360	S355	HEM 400	S355	406.4x16
2		PRS 650x450x32x60		IPE 360		HEM 500		457x12.5
3		PRS 650x450x32x60		IPE 360		HEM 500		457x12.5
4		PRS 650x450x32x60		IPE 360		HEM 450		457x12.5
5		PRS 650x450x32x60		IPE 360		HEM 450		457x12.5
6		PRS 650x450x32x60		IPE 360		HEM 450		457x12.5
7		PRS 650x450x32x60		IPE 360		HEM 400		406.4x12.5
8		PRS 650x450x32x60		IPE 360		HEM 360		355.6x12.5
9		HEM 550		IPE 360		HEM 360		355.6x12.5
10	S460	HEM 550		IPE 360		HEM 340		323.9x12
11		HEM 550		IPE 360		HEM 320		323.9x12
12		HEM 550		IPE 360		HEB 450		323.9x10
13	S355	HEB 300		IPE 360		HEB 400		323.9x10
14		HEB 300		IPE 360		HEB 360		244.5x10
15		HEB 300		IPE 360		HEB 280		193.7x12
16		HEB 300		IPE 360		HEB 220		168.3x10

D-EBF 1.1.1.1.1								
Storey	**Columns**		**Outer Beam**		**Inner Beam/Link**		**Brace**	
[-]	**Material**	**Profile**	**Material**	**Profile**	**Material**	**Profile**	**Material**	**CHS**
1	S460	HEB 240	S355	IPE 330	S355	HEB 240	S355	168.3x10
2		HEB 240		IPE 330		HEB 220		168.3x8
3		HEB 240		IPE 330		HEB 220		168.3x6.3
4		HEB 240		IPE 330		HEB 180		168.3x5
5	S355	HEB 180		IPE 240		HEB 180		168.3x5
6		HEB 180		IPE 240		HEB 180		139.7x8
7		HEB 180		IPE 240		HEB 160		139.7x6
8		HEB 180		HEA 160		HEA 160		139.7x3.6

D-EBF 1.1.1.1.2								
Storey	**Columns**		**Outer Beam**		**Inner Beam/Link**		**Brace**	
[-]	**Material**	**Profile**	**Material**	**Profile**	**Material**	**Profile**	**Material**	**CHS**
1	S460	HEB 280	S355	IPE 300	S355	HEB 240	S355	168.3x10
2		HEB 280		IPE 300		HEB 220		168.3x8
3		HEB 280		IPE 300		HEB 200		168.3x6.3
4		HEB 280		IPE 300		HEB 180		168.3x5
5	S355	HEB 200		IPE 240		HEB 180		168.3x5
6		HEB 200		IPE 240		HEB 180		139.7x8
7		HEB 200		IPE 240		HEB 160		139.7x6
8		HEB 200		HEA 160		HEA 160		139.7x3.6

D-EBF 1.1.1.2.1								
Storey	**Columns**		**Outer Beam**		**Inner Beam/Link**		**Brace**	
[-]	**Material**	**Profile**	**Material**	**Profile**	**Material**	**Profile**	**Material**	**CHS**
1	S460	HEB 300	S355	IPE 360	S355	HEB 360	S355	219.1x10
2		HEB 300		IPE 360		HEB 340		219.1x10
3		HEB 300		IPE 360		HEB 320		193.7x10
4		HEB 300		IPE 360		HEB 300		193.7x10
5	S355	HEB 280		IPE 300		HEB 280		193.7x8
6		HEB 280		IPE 300		HEB 260		168.3x10
7		HEB 280		IPE 300		HEB 200		168.3x6
8		HEB 280		HEB 160		HEB 160		139.7x6

D-EBF 1.1.1.2.2								
Storey	**Columns**		**Outer Beam**		**Inner Beam/Link**		**Brace**	
[-]	**Material**	**Profile**	**Material**	**Profile**	**Material**	**Profile**	**Material**	**CHS**
1	S460	HEB 450	S355	IPE 360	S355	HEB 340	S355	193.7x12
2		HEB 450		IPE 360		HEB 340		193.7x12
3		HEB 450		IPE 360		HEB 320		193.7x10
4		HEB 450		IPE 360		HEB 300		193.7x8
5	S355	HEB 300		IPE 330		HEB 300		193.7x8
6		HEB 300		IPE 330		HEB 240		168.3x8
7		HEB 300		IPE 330		HEB 200		168.3x6
8		HEB 300		HEB 160		HEB 160		139.7x5

D-EBF 1.1.2.1.1								
Storey	**Columns**		**Outer Beam**		**Inner Beam/Link**		**Brace**	
[-]	**Material**	**Profile**	**Material**	**Profile**	**Material**	**Profile**	**Material**	**CHS**
1	S460	HEM 300	S355	HEA 360	S355	HEB 400	S355	244.5x12.5
2		HEM 300		HEA 360		HEB 400		244.5x12.5
3		HEM 300		HEA 360		HEB 360		244.5x10
4		HEM 300		HEA 360		HEB 320		219.1x12
5	S355	HEB 300		IPE 400		HEB 300		219.1x10
6		HEB 300		IPE 400		HEB 280		193.7x12
7		HEB 300		IPE 400		HEB 220		193.7x12
8		HEB 300		HEB 240		HEB 180		168.3x8

D-EBF 1.1.2.1.2								
Storey	**Columns**		**Outer Beam**		**Inner Beam/Link**		**Brace**	
[-]	**Material**	**Profile**	**Material**	**Profile**	**Material**	**Profile**	**Material**	**CHS**
1	S460	HEM 320	S355	HEA 400	S355	HEB 450	S355	273x12
2		HEM 320		HEA 400		HEB 400		244.5x12.5
3		HEM 320		HEA 400		HEB 400		244.5x12.5
4		HEM 320		HEA 400		HEB 340		219.1x12
5	S355	HEB 300		HEA 300		HEB 320		219.1x12
6		HEB 300		HEA 300		HEB 300		197.3x12.5
7		HEB 300		HEA 300		HEB 240		197.3x10
8		HEB 300		HEA 300		HEB 180		197.3x5

D-EBF 1.1.2.2.1								
Storey	**Columns**		**Outer Beam**		**Inner Beam/Link**		**Brace**	
[-]	**Material**	**Profile**	**Material**	**Profile**	**Material**	**Profile**	**Material**	**CHS**
1	S460	HEM 300	S355	HEA 400	S355	HEB 500	S355	273x12.5
2		HEM 300		HEA 400		HEB 500		273x12.5
3		HEM 300		HEA 400		HEB 450		273x12.5
4		HEM 300		HEA 400		HEB 400		244.5x12
5	S355	HEB 300		HEA 340		HEB 400		244.5x12
6		HEB 300		HEA 340		HEB 320		219.1x12
7		HEB 300		HEA 340		HEB 240		193.7x10
8		HEB 300		HEB 240		HEB 180		168.3x8

D-EBF 1.1.2.2.2								
Storey	**Columns**		**Outer Beam**		**Inner Beam/Link**		**Brace**	
[-]	**Material**	**Profile**	**Material**	**Profile**	**Material**	**Profile**	**Material**	**CHS**
1	S460	HEM 340	S355	HEA 400	S355	HEB 450	S355	273x12
2		HEM 340		HEA 400		HEB 400		273x12
3		HEM 340		HEA 400		HEB 400		244.5x12
4		HEM 340		HEA 400		HEB 360		244.5x10
5	S355	HEB 300		IPE 450		HEB 340		244.5x10
6		HEB 300		IPE 450		HEB 300		219.1x10
7		HEB 300		IPE 450		HEB 240		193.7x10
8		HEB 300		HEM 180		HEB 180		168.3x8

D-EBF 1.2.2.1.2								
Storey	**Columns**		**Outer Beam**		**Inner Beam/Link**		**Brace**	
[-]	**Material**	**Profile**	**Material**	**Profile**	**Material**	**Profile**	**Material**	**CHS**
1	S690	PRS 250x300x18x30	S355	HEA 400	S355	HEB 400	S355	244.5x12.5
2		PRS 250x300x18x30		HEA 400		HEB 360		244.5x12.5
3		PRS 250x300x18x30		HEA 400		HEB 340		219.1x12.5
4		PRS 250x300x18x30		HEA 400		HEB 320		219.1x12.5
5	S355	HEB 300		IPE 400		HEB 300		219.1x10
6		HEB 300		IPE 400		HEB 280		197.3x12
7		HEB 300		IPE 400		HEB 220		197.3x8
8		HEB 300		HEM 180		HEB 180		168.3x8

D-EBF 1.2.2.2.2								
Storey	**Columns**		**Outer Beam**		**Inner Beam/Link**		**Brace**	
[-]	**Material**	**Profile**	**Material**	**Profile**	**Material**	**Profile**	**Material**	**CHS**
1	S690	PRS 250x300x18x38	S355	HEA 400	S355	HEB 450	S355	323.9x12
2		PRS 250x300x18x38		HEA 400		HEB 400		323.9x12
3		PRS 250x300x18x38		HEA 400		HEB 400		273x12
4		PRS 250x300x18x38		HEA 400		HEB 360		244.5x12
5	S355	HEB 300		IPE 400		HEB 340		244.5x12
6		HEB 300		IPE 400		HEB 300		219.1x10
7		HEB 300		IPE 400		HEB 240		193.7x10
8		HEB 300		HEM 180		HEB 180		168.3x8

D-EBF 2.1.2.1.1								
Storey	**Columns**		**Outer Beam**		**Inner Beam/Link**		**Brace**	
[-]	**Material**	**Profile**	**Material**	**Profile**	**Material**	**Profile**	**Material**	**CHS**
1	S460	PRS 600x400x20x55	S355	HEA 500	S355	HEM 360	S355	355.6x12.5
2		PRS 600x400x20x55		HEA 500		HEM 500		457x12.5
3		PRS 600x400x20x55		HEA 500		HEM 450		457x12
4		PRS 600x400x20x55		HEA 500		HEM 400		406.4x12.5
5		HEM 600		HEA 450		HEM 360		355.6x12.5
6		HEM 600		HEA 450		HEM 340		355.6x12.5
7		HEM 600		HEA 450		HEM 300		323.9x12
8		HEM 600		HEA 450		HEB 450		323.9x12
9		HEB 450		IPE 500		HEB 450		273x12
10		HEB 450		IPE 500		HEB 400		244.5x12.5
11		HEB 450		IPE 500		HEB 400		244.5x12.5
12		HEB 450		IPE 500		HEB 360		244.5x12
13	S355	HEB 300		IPE 450		HEB 360		244.5x12
14		HEB 300		IPE 450		HEB 320		219.1x12
15		HEB 300		IPE 450		HEB 260		193.7x12
16		HEB 300		HEB 240		HEB 200		193.7x6

D-EBF 2.1.2.1.2								
Storey	**Columns**		**Outer Beam**		**Inner Beam/Link**		**Brace**	
[-]	**Material**	**Profile**	**Material**	**Profile**	**Material**	**Profile**	**Material**	**CHS**
1	S460	PRS 680x450x30x50	S355	HEA 500	S355	HEB 500	S355	355.6x12
2		PRS 680x450x30x50		HEA 500		HEM 450		457x12
3		PRS 680x450x30x50		HEA 500		HEM 400		406.4x12.5
4		PRS 680x450x30x50		HEA 500		HEM 360		406.4x12
5		PRS 600x400x20x30		HEA 450		HEM 340		355.6x12.5
6		PRS 600x400x20x30		HEA 450		HEM 340		355.6x12
7		PRS 600x400x20x30		HEA 450		HEM 300		323.9x12
8		PRS 600x400x20x30		HEA 450		HEB 400		273x12.5
9		HEB 500		HEA 400		HEB 450		273x12.5
10		HEB 500		HEA 400		HEB 400		273x12
11		HEB 500		HEA 400		HEB 360		273x10
12		HEB 500		HEA 400		HEB 340		244.5x12
13	S355	HEB 300		IPE 450		HEB 360		244.5x12
14		HEB 300		IPE 450		HEB 320		219.1x12
15		HEB 300		IPE 450		HEB 260		219.1x8
16		HEB 300		HEB 240		HEB 200		193.7x6

D-EBF 2.1.2.2.1								
Storey	**Columns**		**Outer Beam**		**Inner Beam/Link**		**Brace**	
[-]	**Material**	**Profile**	**Material**	**Profile**	**Material**	**Profile**	**Material**	**CHS**
1	S460	PRS 830x470x35x75	S355	HEB 600	S355	HEM 650	S355	457x16
2		PRS 830x470x35x75		HEB 600		HEM 800		457x20
3		PRS 830x470x35x75		HEB 600		HEM 800		457x20
4		PRS 830x470x35x75		HEB 600		HEM 650		406.4x20
5		PRS 750x450x20x40		HEB 550		HEM 650		406.4x20
6		PRS 750x450x20x40		HEB 550		HEM 650		406.4x20
7		PRS 750x450x20x40		HEB 550		HEM 550		406.4x16
8		PRS 750x450x20x40		HEB 550		HEM 500		406.4x16
9		HEB 650		HEB 500		HEM 500		406.4x16
10		HEB 650		HEB 500		HEM 450		355.6x16
11		HEB 650		HEB 500		HEM 400		323.9x16
12		HEB 650		HEB 500		HEM 300		323.9x12
13	S355	HEB 300		HEA 400		HEM 320		273x16
14		HEB 300		HEA 400		HEB 400		273x12
15		HEB 300		HEA 400		HEB 320		219.1x12
16		HEB 300		HEB 240		HEB 220		193.7x8

D-EBF 2.1.2.2.2								
Storey	**Columns**		**Outer Beam**		**Inner Beam/Link**		**Brace**	
[-]	**Material**	**Profile**	**Material**	**Profile**	**Material**	**Profile**	**Material**	**CHS**
1	S460	PRS 800x500x34x75	S355	IPE 360	S355	HEM 400	S355	406.4x16
2		PRS 800x500x34x75		IPE 360		HEM 500		457x12
3		PRS 800x500x34x75		IPE 360		HEM 500		457x12
4		PRS 800x500x34x75		IPE 360		HEM 500		457x12
5		PRS 700x450x22x50		IPE 360		HEM 450		457x12
6		PRS 700x450x22x50		IPE 360		HEM 450		457x12
7		PRS 700x450x22x50		IPE 360		HEM 450		406.4x12.5
8		PRS 700x450x22x50		IPE 360		HEM 400		355.6x12.5
9		HEM 600		IPE 360		HEM 400		355.6x12.5
10		HEM 600		IPE 360		HEM 360		323.9x12.5
11		HEM 600		IPE 360		HEM 360		323.9x12.5
12		HEM 600		IPE 360		HEB 450		323.9x10
13	S355	HEB 300		IPE 360		HEB 400		323.9x10
14		HEB 300		IPE 360		HEB 360		244.5x10
15		HEB 300		IPE 360		HEB 300		219.1x10
16		HEB 300		IPE 360		HEB 220		168.3x10

D-EBF 2.2.2.1.2								
Storey	**Columns**		**Outer Beam**		**Inner Beam/Link**		**Brace**	
[-]	**Material**	**Profile**	**Material**	**Profile**	**Material**	**Profile**	**Material**	**CHS**
1	S690	PRS 680x425x20x45	S355	IPE 360	S355	HEB 360	S355	355.6x10
2		PRS 680x425x20x45		IPE 360		HEM 360		457x10
3		PRS 680x425x20x45		IPE 360		HEM 340		406.4x10
4		PRS 680x425x20x45		IPE 360		HEM 320		406.4x10
5		PRS 550x350x15x35		IPE 360		HEM 300		355.6x10
6		PRS 550x350x15x35		IPE 360		HEM 300		355.6x10
7		PRS 550x350x15x35		IPE 360		HEB 450		323.9x10
8		PRS 550x350x15x35		IPE 360		HEB 400		273x12
9	S460	HEM 300		IPE 360		HEB 400		273x12
10		HEM 300		IPE 360		HEB 400		273x10
11		HEM 300		IPE 360		HEB 360		273x10
12		HEM 300		IPE 360		HEB 340		244.5x10
13	S355	HEB 300		IPE 360		HEB 340		244.5x10
14		HEB 300		IPE 360		HEB 300		219.1x10
15		HEB 300		IPE 360		HEB 240		193.7x10
16		HEB 300		IPE 360		HEB 200		193.7x6

D-EBF 2.2.2.2.2								
Storey	**Columns**		**Outer Beam**		**Inner Beam/Link**		**Brace**	
[-]	**Material**	**Profile**	**Material**	**Profile**	**Material**	**Profile**	**Material**	**CHS**
1	S690	PRS 650x450x32x60	S355	IPE 360	S355	HEM 400	S355	406.4x16
2		PRS 650x450x32x60		IPE 360		HEM 500		457x12.5
3		PRS 650x450x32x60		IPE 360		HEM 500		457x12.5
4		PRS 650x450x32x60		IPE 360		HEM 450		457x12.5
5		PRS 650x450x32x60		IPE 360		HEM 450		457x12.5
6		PRS 650x450x32x60		IPE 360		HEM 450		457x12.5
7		PRS 650x450x32x60		IPE 360		HEM 400		406.4x12.5
8		PRS 650x450x32x60		IPE 360		HEM 360		355.6x12.5
9		HEM 550		IPE 360		HEM 360		355.6x12.5
10	S460	HEM 550		IPE 360		HEM 340		323.9x12
11		HEM 550		IPE 360		HEM 320		323.9x12
12		HEM 550		IPE 360		HEB 450		323.9x10
13	S355	HEB 300		IPE 360		HEB 400		323.9x10
14		HEB 300		IPE 360		HEB 360		244.5x10
15		HEB 300		IPE 360		HEB 280		193.7x12
16		HEB 300		IPE 360		HEB 220		168.3x10